

## CANCER

# PI4KIII $\beta$ is a therapeutic target in chromosome 1q-amplified lung adenocarcinoma

Xiaochao Tan<sup>1\*</sup>, Priyam Banerjee<sup>1\*</sup>, Edward A. Pham<sup>2\*</sup>, Florentine U. N. Rutaganira<sup>3</sup>, Kaustabh Basu<sup>2</sup>, Neus Bota-Rabassedas<sup>1</sup>, Hou-Fu Guo<sup>1</sup>, Caitlin L. Grzeskowiak<sup>4,5</sup>, Xin Liu<sup>1</sup>, Jiang Yu<sup>1</sup>, Lei Shi<sup>1</sup>, David H. Peng<sup>1</sup>, B. Leticia Rodriguez<sup>1</sup>, Jiaqi Zhang<sup>1</sup>, Veronica Zheng<sup>1</sup>, Dzifa Y. Duose<sup>6</sup>, Luisa M. Solis<sup>6</sup>, Barbara Mino<sup>6</sup>, Maria Gabriela Raso<sup>6</sup>, Carmen Behrens<sup>6</sup>, Ignacio I. Wistuba<sup>6</sup>, Kenneth L. Scott<sup>4,5</sup>, Mark Smith<sup>2,7</sup>, Khanh Nguyen<sup>2</sup>, Grace Lam<sup>2</sup>, Ingrid Choong<sup>2</sup>, Abhijit Mazumdar<sup>8</sup>, Jamal L. Hill<sup>8</sup>, Don L. Gibbons<sup>1</sup>, Powell H. Brown<sup>8</sup>, William K. Russell<sup>9</sup>, Kevan Shokat<sup>3</sup>, Chad J. Creighton<sup>5,10†</sup>, Jeffrey S. Glenn<sup>2,11†</sup>, Jonathan M. Kurie<sup>1†</sup>

Copyright © 2020  
The Authors, some  
rights reserved;  
exclusive licensee  
American Association  
for the Advancement  
of Science. No claim  
to original U.S.  
Government Works

Heightened secretion of protumorigenic effector proteins is a feature of malignant cells. Yet, the molecular underpinnings and therapeutic implications of this feature remain unclear. Here, we identify a chromosome 1q region that is frequently amplified in diverse cancer types and encodes multiple regulators of secretory vesicle biogenesis and trafficking, including the Golgi-dedicated enzyme phosphatidylinositol (PI)-4-kinase III $\beta$  (PI4KIII $\beta$ ). Molecular, biochemical, and cell biological studies show that PI4KIII $\beta$ -derived PI-4-phosphate (PI4P) synthesis enhances secretion and accelerates lung adenocarcinoma progression by activating Golgi phosphoprotein 3 (GOLPH3)-dependent vesicular release from the Golgi. PI4KIII $\beta$ -dependent secreted factors maintain 1q-amplified cancer cell survival and influence prometastatic processes in the tumor microenvironment. Disruption of this functional circuitry in 1q-amplified cancer cells with selective PI4KIII $\beta$  antagonists induces apoptosis and suppresses tumor growth and metastasis. These results support a model in which chromosome 1q amplifications create a dependency on PI4KIII $\beta$ -dependent secretion for cancer cell survival and tumor progression.

## INTRODUCTION

The tumor stroma is rich in factors that play key roles in metastasis (1). Chemokines, cytokines, and growth factors promote inflammation and angiogenesis and increase the proliferative and invasive properties of cancer cells (1). Collagen proteases and cross-linking enzymes remodel collagen fibers to increase stromal stiffness, enhance cancer cell invasion, and restrict the influx of antitumor immune cells (2). Thus far, clinical trials targeting secreted peptides in the tumor microenvironment such as matrix metalloproteinases (MMPs) and vascular endothelial growth factors have not demonstrated robust antitumor activity (3). Potential contributors to these outcomes include functional redundancies within the secretory network, physical and/or biochemical barriers in tumor stroma that reduce drug bioavailability, and de novo drug resistance (4, 5). Moreover, the way in which malignant secretion is activated in cancer remains

unclear. Addressing this knowledge gap may lead to improved therapeutic approaches.

Proteins secreted through the conventional secretory pathway are transported as vesicular cargos from the endoplasmic reticulum to the cell surface via the Golgi apparatus (6). Vesicular biogenesis in the Golgi is driven by Golgi phosphoprotein 3 (GOLPH3), which bridges Golgi membranes to F-actin fibers that convey a tensile force required for vesicular budding and release (7). GOLPH3 is tethered to Golgi membranes by phosphatidylinositol (PI) 4-phosphate (PI4P) generated by the Golgi-resident PI-4-kinases PI4KII $\alpha$  and PI4KIII $\beta$  (7, 8). Conversely, the PI4P phosphatase SAC-1 impedes vesicle biogenesis by shuttling reversibly between the endoplasmic reticulum and the Golgi apparatus to create a PI4P gradient across the Golgi stack (9). The genes encoding GOLPH3 and phosphatidylinositol transfer protein cytoplasmic 1 (PITPNM1), a PI4P-binding protein that facilitates the recruitment of GOLPH3 to the Golgi, reside on chromosomal amplifications found in multiple epithelial cancer types (8). High GOLPH3 and PITPNM1 increase the secretion of proteins that drive tumor growth and metastasis (8, 10). On the basis of this conceptual framework, here, we evaluated the conventional secretory pathway for therapeutic targets and found that Golgi-resident PI4P synthesis drives malignant secretion and underlies an actionable secretory vulnerability in a molecularly defined subset of cancers.

## RESULTS

## A chromosome 1q amplicon links Golgi-related functions to metastasis

By using the Gene Ontology term “Golgi apparatus” to interrogate The Cancer Genome Atlas (TCGA) database, we identified a chromosomal amplification that consistently involves a 1q21.3 region and variable segments of a much broader region (1q21–43) in numerous

<sup>1</sup>Department of Thoracic/Head and Neck Medical Oncology, The University of Texas MD Anderson Cancer Center, Houston, TX 77030, USA. <sup>2</sup>Departments of Medicine and Microbiology & Immunology, Division of Gastroenterology and Hepatology, Stanford University School of Medicine, Stanford, CA 94305, USA. <sup>3</sup>Howard Hughes Medical Institute and Department of Cellular and Molecular Pharmacology, University of California, San Francisco, San Francisco, CA 94143, USA. <sup>4</sup>Department of Molecular and Human Genetics, Dan L. Duncan Cancer Center, Baylor College of Medicine, Houston, TX 77030, USA. <sup>5</sup>Department of Medicine, Dan L. Duncan Cancer Center, Baylor College of Medicine, Houston, TX 77030, USA. <sup>6</sup>Department of Translational Molecular Pathology, The University of Texas MD Anderson Cancer Center, Houston, TX 77030, USA. <sup>7</sup>Stanford ChEM-H Medicinal Chemistry Knowledge Center, Stanford University, CA 94305, USA. <sup>8</sup>Department of Cancer Prevention, The University of Texas MD Anderson Cancer Center, Houston, TX 77030, USA. <sup>9</sup>Department of Biochemistry and Molecular Biology, University of Texas Medical Branch, Galveston, TX 77555, USA. <sup>10</sup>Department of Bioinformatics and Computational Biology, The University of Texas MD Anderson Cancer Center, Houston, TX 77030, USA. <sup>11</sup>Veterans Administration Medical Center, Palo Alto, CA 94304, USA.

\*These authors contributed equally to this work.

†Corresponding author. Email: jkurie@mdanderson.org (J.M.K.); jeffrey.glen@stanford.edu (J.S.G.); creighto@bcm.edu (C.J.C.)

tumor types, including fractions of breast (13%), lung (14%), and ovarian (12%) adenocarcinomas (Fig. 1A). The 1q21-43 region encodes genes that control Golgi organelle integrity (*GPR89A*, *COPA*, *ACBD3*, *ARF1*, and *COG2*), intra-Golgi protein modifications (*GALNT2*), ion transport (*GPR89A*), nicotinamide adenine dinucleotide synthesis (*NMNAT2*), vesicular biogenesis (*PI4KB*, *GOLPH3L*, *COPA*, *ACBD3*, and *ARF1*), and vesicular trafficking (*VPS45*, *BLZF-1/Golgin-45*, *GOLT1A*, *RAB13*, *SCAMP3*, *TMEM79*, *VAMP4*, *KLHL20*, *STX6*, *RAB7L1*, *ARF1*, and *CNST*) (Fig. 1A) (11–29). In the TCGA lung adenocarcinoma cohort, 1q-encoded Golgi-related genes are coamplified, and *PI4KB* gene copy numbers are correlated with *PI4KB* mRNA amounts (Fig. 1, B and C). *PI4KB* gene amplifications co-occur with *GOLPH3* and *PITPNM1* amplifications (Fig. 1D), which are critical mediators of PI4KIII $\beta$ -dependent secretion (8), whereas amplifications of other PI4K family members are rare (Fig. 1E). In a human lung adenocarcinoma cell line panel annotated for the presence or absence of 1q amplifications [COSMIC (Catalogue Of Somatic Mutations In Cancer), [https://cancer.sanger.ac.uk/cell\\_lines](https://cancer.sanger.ac.uk/cell_lines); cBioPortal, [www.cbiopal.org](http://www.cbiopal.org)], 1q-encoded gene copy numbers are correlated with their respective mRNA and protein amounts (Fig. 1F and fig. S1). PI4P concentrations were higher in 1q-amplified than in 1q-diploid lung cancer cell lines (Fig. 1G). These findings suggest “priming” of the conventional secretory pathway in 1q-amplified lung cancer cells.

Higher expression of a signature composed of all genes in the recurrently amplified 1q21.3 region is associated with a worse prognosis in the TCGA lung adenocarcinoma cohort (Fig. 1H). To determine whether PI4KIII $\beta$  is an important driver of this association, we used a digital droplet polymerase chain reaction (PCR) approach to quantify *PI4KB* copy numbers. The specificity of this assay was validated on genomic DNA from a 1q-amplified lung adenocarcinoma cell line (H3122) and 1q-diploid normal human lung tissues (Fig. 1I). To investigate the clinical relevance of increased *PI4KB* copy numbers, we procured tumor genomic DNA samples from a cohort of clinically annotated early-stage lung adenocarcinoma specimens ( $n = 89$ ) (table S1). *PI4KB* copy numbers were calculated from *PI4KB* PCR values normalized on the basis of a reference gene (*RPP30*) and expressed as a ratio of tumor-to-normal lung. A cutoff value of  $\geq 3.5$  copies was used to define *PI4KB*-amplified tumors. *PI4KB* amplifications, which were identified in 12 (13%) of 89 tumor specimens, were correlated with increased *PI4KB* mRNA expression (Fig. 1J), shorter survival durations ( $P < 0.001$ , log-rank test) (Fig. 1K), and increased rate of disease recurrence ( $P = 0.03$ ; odds ratio = 5.4, Fisher’s  $\chi^2$  test) (Fig. 1L). In corroboration, high *PI4KB* mRNA expression was associated with a worse prognosis in the same cohort (Fig. 1M).

To investigate the biological roles of 1q-encoded Golgi-related genes, we introduced small interfering RNAs (siRNAs) into 1q-amplified lung adenocarcinoma cells, focusing initially on genes in the recurrently amplified 1q21.3 region (fig. S2A). Relative to the effects of control siRNA, siRNAs against PI4KIII $\beta$ , RAB13, or VPS45 reduced the colony-forming activities of H2122 cells (fig. S2, B and C). H2122 cell proliferation in monolayer culture was impaired only by PI4KIII $\beta$  siRNAs (fig. S2D). Similarly, PI4KIII $\beta$  siRNAs attenuated the proliferative, colony-forming, and migratory and invasive activities of 1q-amplified H23 and H3122 lung cancer cells (fig. S2, E to J) and 1q-amplified breast and ovarian adenocarcinoma cell lines (fig. S3). GOLPH3L siRNAs had no detectable effect in any of the assays (fig. S2, B to J), which is consistent with evidence that GOLPH3L antagonizes GOLPH3-dependent vesicular trafficking (16). Thus,

1q21.3-encoded Golgi-related genes play important roles in 1q-amplified tumor cells.

The finding that the 1q amplicon harbors multiple regulators of vesicle biogenesis and trafficking led us to speculate that the coamplified genes function cooperatively. To address this possibility, we subjected a 1q-diploid lung cancer cell line (H1299) to ectopic expression of PI4KIII $\beta$  alone or in combination with a coamplified gene (fig. S4A) and examined the invasive activities of the transfectants in Boyden chambers. Relative to the effects of ectopic PI4KIII $\beta$  expression alone, invasion was enhanced by coexpression of *GPR89A*, *ACBD3*, *TMEM79*, *VANGL2*, *VAMP4*, or *ARF1* (fig. S4, B and C). *ACBD3* is a scaffolding protein required for the recruitment of PI4KIII $\beta$  to Golgi membranes (30), and *GPR89A* is an anion channel that drives Golgi lumen acidification, which is crucial for cargo protein glycosylation, processing, and trafficking (31, 32). To examine functional interactions between these genes in greater detail, murine *Kras/Trp53*-mutant lung adenocarcinoma (KP) cells (33) were subjected to ectopic expression of PI4KIII $\beta$  alone or in combination with *ACBD3* or *GPR89A* (fig. S4D), and the transfectants were injected into syngeneic, immunocompetent mice, which showed that PI4KIII $\beta$ -driven tumor growth and metastatic activity were enhanced by coexpression of *ACBD3* or *GPR89A* (fig. S4E).

### PI4KIII $\beta$ accelerates *KRAS*-mutant lung adenocarcinoma progression

In the TCGA lung adenocarcinoma cohort, *PI4KB* copy number gains co-occurred with point mutations in *KRAS* and point mutations or gene fusions involving multiple receptor tyrosine kinases (EGFR, ALK, RET, and MET) (Fig. 2A), indicating that *PI4KB* amplifications arise in the context of a variety of oncogenic driver mutations. The relatively high frequency with which *PI4KB* amplifications co-occur with *KRAS* mutations led us to ask whether high PI4KIII $\beta$  expression accelerates *KRAS*-mutant lung adenocarcinoma progression. To address this question, we delivered lentiviruses that coexpress Cre and PI4KIII $\beta$  (lenti-CP) or Cre and green fluorescence protein (lenti-CG) (Fig. 2B) by intratracheal aerosol to *Kras*<sup>LSL-G12D</sup> mice, which develop nonmetastatic lung adenocarcinomas after Cre-mediated recombination of a *Kras*<sup>LOX-STOP-LOX-G12D</sup>(*Kras*<sup>LSL-G12D</sup>) allele (34). Lentivirus-infected mice were subjected to serial micro-computed tomography (CT) (Fig. 2C) to quantify changes in lung tumor size over time, which showed a faster tumor growth rate in lenti-CP– than in lenti-CG–infected mice (Fig. 2, D to F). Necropsies were performed 5 months after lentiviral delivery, which coincided with the development of early lung neoplasia (adenomas) (34). PCR analysis confirmed Cre-mediated recombination of the *Kras*<sup>LSL-G12D</sup> allele in tumor tissues (Fig. 2G). PI4KIII $\beta$  detected immunohistochemically in tumors (Fig. 2H) was digitally scanned and scored on the basis of staining intensity and extent, which showed that intratumoral PI4KIII $\beta$  expression was higher in lenti-CP– than in lenti-CG–infected mice (mean values, 161.8 versus 118.4, respectively). Lung tumors were histologically confirmed in 7 (70%) of 10 lenti-CG–infected mice and 8 (72.7%) of 11 lenti-CP–infected mice. Although adenomas and adenocarcinomas (Fig. 2, I and J) were identified in both cohorts, adenocarcinomas were significantly more numerous in the lenti-CP cohort [7 (100%) of 7 versus 2 (25%) of 8] ( $P = 0.002$ ), indicating that high PI4KIII $\beta$  expression accelerated adenocarcinoma development. Distant metastases were not identified in either cohort, which was expected given that mice were necropsied at an early time point (20 weeks). To more fully examine the prometastatic activity of

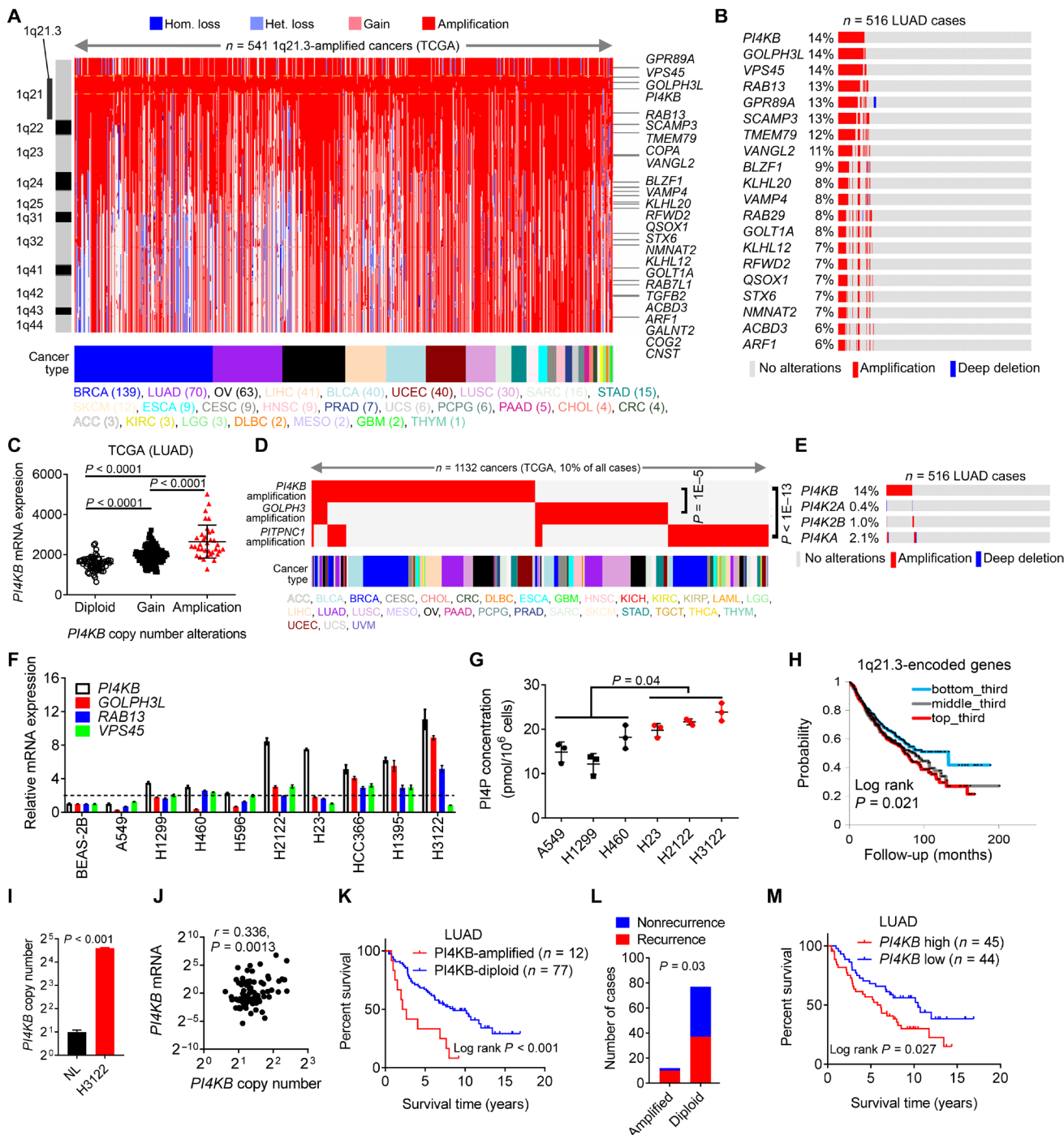


**Fig. 1. A chromosome 1q region encoding multiple Golgi-related genes is amplified in cancer.** (A) Heat map of copy number alterations in 1038 genes (rows) in 1q21.3-amplified cancers (n = 541, columns) in The Cancer Genome Atlas (TCGA) cohort. 1q21–44-encoded genes annotated under the Gene Ontology term Golgi apparatus (right). Color codes for tumor types (bottom of heat map) and copy number changes (top) are indicated. (B) Copy number variations of genes (rows) in TCGA lung adenocarcinomas (columns). (C) PI4KB gene copy number alterations (x axis) and relative mRNA expression (y axis) in TCGA lung adenocarcinomas (n = 522). Gain, n = 3 to 4 copies; amplified, n ≥ 5 copies. (D and E) Somatic mutations (rows) in TCGA pan-cancer (D) and lung adenocarcinoma (E) cohorts (columns). (F) Relative expression of 1q21.3-encoded mRNAs in lung cancer cell lines with or without 1q21.3 amplifications. Immortalized bronchial epithelial (BEAS-2B) cells included as control. (G) Total cellular PI4P concentrations in 1q-amplified (red) and 1q-diploid (black) lung cancer cell lines determined by enzyme-linked immunosorbent assay (ELISA). Each dot is a replicate sample. (H) Kaplan-Meier plot comparing groups with high (top-third), intermediate (middle-third), or low (bottom-third) expression of a 1q21.3-encoded gene expression signature. (I) Digital droplet PCR analysis of PI4KB copy numbers in normal lung (NL) tissues and 1q-amplified H3122 lung adenocarcinoma cells. (J) PI4KB copy numbers (x axis) and mRNA expression (y axis) in human lung adenocarcinomas (dots) (r and P values, Pearson's correlation). (K) Kaplan-Meier plot comparing groups with or without PI4KB genomic amplifications. (L) Tumor recurrence rates in PI4KB-amplified and PI4KB-diploid human lung adenocarcinomas. (M) Kaplan-Meier plot comparing groups with PI4KB mRNA expression above (high) or below (low) the median value.

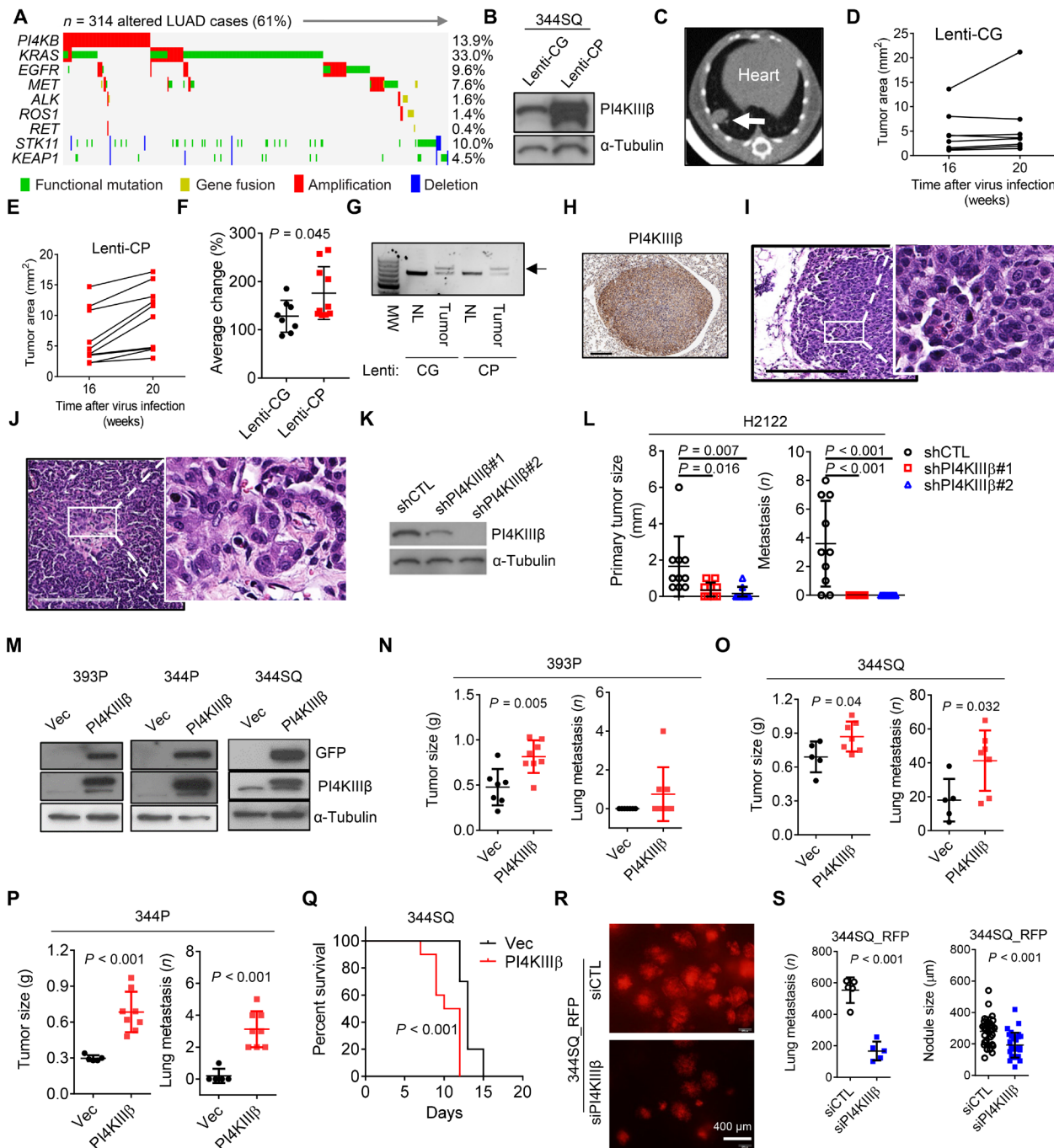


**Fig. 2. PI4KIII $\beta$  functions as a metastasis driver in KRAS-mutant lung adenocarcinoma.** (A) Co-occurrence of somatic mutations (rows) in TCGA lung adenocarcinomas (columns). (B) Western blot analysis of lentivirus-infected 344SQ cells. (C) Micro-CT of a lung tumor (arrow) in a *Kras*<sup>LSL-G12D</sup> mouse. (D and E) Area of each lung tumor in the lenti-CG (black dots) and lenti-CP (red squares) cohorts determined by micro-CT. (F) Percent change in tumor areas over time. (G) PCR analysis of genomic DNA from normal lung and lung tumor. Recombined *Kras*<sup>LSL-G12D</sup> allele (arrow). Molecular weight (MW) markers. (H) Immunohistochemical detection of PI4KIII $\beta$  in a lung tumor in a lenti-CP-infected mouse. Scale bar, 200  $\mu\text{m}$ . (I and J) Lung adenoma (I) and adenocarcinoma (J). Boxed areas are shown at higher magnification (insets). Scale bar, 200  $\mu\text{m}$ . (K) Western blot analysis of H2122 cells transfected with indicated PI4KIII $\beta$  shRNAs or control shRNA (shCTL). (L) Orthotopic tumor diameters (left) and number of metastases to contralateral lung (right) per mouse (dot). (M) Western blot analysis of ectopic PI4KIII $\beta$  expression in murine KP cell lines. Vec, empty vector. (N to P) Flank tumor weights and lung metastasis numbers (left and right, respectively) generated from 393P (N), 344SQ (O), and 344P (P) KP cell lines per mouse (dots). (Q) Kaplan-Meier plot of mouse cohorts bearing orthotopic tumors. (R and S) Red fluorescent protein (RFP)-tagged 344SQ cells were injected by tail vein into mice, and lung tumors (red) were visualized by fluorescence microscopy of intact lung tissues (R) and quantified (dots) based on numbers (left) and size (S). Scale bar, 400  $\mu\text{m}$ .

PI4KIII $\beta$  in *KRAS*-mutant lung adenocarcinomas, we injected nude mice with *KRAS*-mutant H2122 cells that are PI4KIII $\beta$  deficient or replete (Fig. 2K) and found that PI4KIII $\beta$ -deficient H2122 cells generated smaller and less metastatic tumors (Fig. 2L). Furthermore, the growth and metastatic activities of tumors generated by KP cells (393P, 344P, and 344SQ) in syngeneic, immunocompetent mice were enhanced by ectopic PI4KIII $\beta$  expression (Fig. 2, M to Q) and reduced by PI4KIII $\beta$  depletion (Fig. 2, R and S). Thus, high PI4KIII $\beta$  expression accelerated *KRAS*-mutant lung adenocarcinoma progression.

### PI4KIII $\beta$ is an actionable target in 1q-amplified cancers

Small molecules that bind to the PI4KIII $\beta$  active site and inhibit PI4KIII $\beta$  catalytic activity with greater than 1000-fold selectivity over a panel of class I and class III PI-3-kinase family members demonstrate efficacy against single-stranded RNA viruses that require PI4KIII $\beta$  for replication (35, 36). To determine whether the 1q amplicon confers vulnerability to PI4KIII $\beta$  antagonism, we treated a panel of 1q-amplified and 1q-diploid lung cancer cell lines with the PI4KIII $\beta$  antagonist IN-9 (35). After IN-9 treatment, total cellular PI4P and Golgi-resident PI4P decreased (Fig. 3, A to C). Golgi-resident PI4P decreased similarly after siRNA-mediated PI4KIII $\beta$  depletion (Fig. 3D). Cell proliferation, anchorage-dependent and anchorage-independent colony formation, and cell migration and invasion decreased to a greater extent in 1q-amplified than in 1q-diploid lung cancer cells (Fig. 3, E to I). Apoptosis was detected almost exclusively in 1q-amplified cells (Fig. 3J and fig. S5). IN-9 treatment increased apoptosis more prominently in ectopic PI4KIII $\beta$ -expressing H1299 cells than it did in control transfectants (Fig. 3K), suggesting a causal relationship between heightened PI4KIII $\beta$  expression and IN-9-induced apoptosis.

PI4KIII $\beta$  inhibitors with improved pharmacologic properties were synthesized and designated compounds A and B (fig. S6, A and B). After treatment with these compounds, cell proliferation, colony formation, and cell migration and invasion decreased to a greater extent in 1q-amplified than in 1q-diploid lung cancer cells, and apoptosis was detected only in 1q-amplified cells (Fig. 4, A to J, and fig. S6, C to H). We treated nude mice bearing H2122 orthotopic lung tumors with twice-daily intraperitoneal injection of vehicle or compound A (100 mg/kg) beginning 28 days after tumor cell injection when metastases to the contralateral lung and other sites were established. Mice exhibited no signs of morbidity or weight loss during treatment (fig. S6I). After 7 days of treatment, mice were necropsied for determination of primary tumor size and the number of distant metastases. Relative to controls, compound A-treated mice had smaller primary tumors and fewer metastases to the contralateral lung (Fig. 4K). Compound A also demonstrated efficacy against H23 orthotopic lung tumors (Fig. 4L), 1q-amplified lung adenocarcinoma patient-derived xenografts (Fig. 4M), and 1q-amplified MDA-MB-468 mammary tumors (Fig. 4N). A 21-day treatment with compound B [20 or 40 mg/kg plus ritonavir (20 mg/kg) to improve resistance of compound B to metabolic breakdown] administered subcutaneously twice daily caused no weight loss and exerted dose-dependent activity against H2122 orthotopic tumors (Fig. 4O and fig. S6J). Thus, 1q-amplified cancers are vulnerable to PI4KIII $\beta$  antagonism.

### PI4KIII $\beta$ antagonism blocks Golgi secretory functions

We sought to elucidate the way in which PI4KIII $\beta$  antagonism suppresses tumor growth and metastasis. In addition to generating PI4P (9), PI4KIII $\beta$  has noncatalytic roles that rely on interactions with

other proteins such as RAB11 (25). To determine whether PI4P synthesis is required for PI4KIII $\beta$ -dependent biological effects, we dephosphorylated PI4P in the Golgi by ectopically expressing a mutant SAC-1 phosphatase (SAC1-K2A) that localizes constitutively in the Golgi and dephosphorylates Golgi-resident PI4P (37). SAC1-K2A localized in the Golgi, decreased PI4P, and reduced the proliferation and colony formation of 1q-amplified H2122 cells (Fig. 5, A to D, and fig. S7A). The biological effects of SAC1-K2A were greater in H1299 cells that have ectopic PI4KIII $\beta$  expression than they were in parental H1299 cells or other 1q-diploid lung cancer cells (Fig. 5, E to G, and fig. S7, B to F). To directly examine the role of PI4KIII $\beta$ 's catalytic activity, we ectopically expressed wild-type or kinase-dead mutant PI4KIII $\beta$  in 1q-diploid H1299 cells and PI4KIII $\beta$ -depleted H2122 cells, which showed that PI4P concentration, cell proliferation, colony formation, cell migration and invasion, and tumor growth and metastasis were rescued only by wild-type PI4KIII $\beta$  (Fig. 5, H to R). IN-9 treatment reduced total PI4P concentrations more sharply in ectopic PI4KIII $\beta$ -expressing H1299 cells than it did in control transfectants (fig. S7G), suggesting that PI4KIII $\beta$  is a key driver of Golgi-resident PI4P synthesis in the setting of heightened PI4KIII $\beta$  expression. In contrast, depletion of PI4KII $\alpha$ , which also generates Golgi-resident PI4P (38), reduced 1q-amplified cell proliferation, migration, and invasion but did not significantly increase apoptosis (fig. S7, H to L), suggesting a selective role for PI4KIII $\beta$ -dependent PI4P synthesis in maintaining 1q-amplified lung cancer cell survival.

Having shown that catalytic activity is required for PI4KIII $\beta$ 's prometastatic functions, we then sought to identify PI4P-binding proteins that mediate the cellular functions of PI4KIII $\beta$ . PI4P is the Golgi membrane insertion site for PTPNC1, GOLPH3, and oxysterol-binding proteins that regulate intra-Golgi lipid transport and are essential for vesicle biogenesis (9). In the TCGA lung adenocarcinoma cohort, *GOLPH3* is amplified more frequently than any other genes encoding PI4P-binding Golgi proteins (fig. S8A). We performed siRNA-mediated depletion experiments and found that *GOLPH3* depletion reduced cell proliferation, colony formation, migration, and invasion (fig. S8, B to J), whereas depletion of PI4P-binding lipid transporters had no detectable effect (fig. S8, K to M). To investigate the role of *GOLPH3* in greater detail, we transfected H23 cells with a temperature-sensitive mutant vesicular stomatitis virus (VSV-G) that accumulates in the Golgi at a restrictive temperature and is released for anterograde trafficking at a permissive temperature (39). Compared to controls, siPI4KIII $\beta$ -transfected H23 cells accumulated less VSV-G on the plasma membrane (Fig. 6, A and B). Similar reductions in plasma membrane-bound VSV-G were observed after compound B treatment (Fig. 6C) or siRNA-mediated *GOLPH3* depletion (Fig. 6D). Thus, *GOLPH3* mediates PI4KIII $\beta$ 's prometastatic secretory functions.

### PI4KIII $\beta$ -dependent secretion maintains 1q-amplified cancer cell viability

Next, we sought to identify PI4KIII $\beta$ -dependent secreted proteins that maintain 1q-amplified lung cancer cell survival. Loss of colony formation induced by PI4KIII $\beta$  deficiency was reversed by the addition of conditioned medium from PI4KIII $\beta$ -replete, but not PI4KIII $\beta$ -deficient, H2122 cells (Fig. 6E), and apoptosis induced by treatment with the PI4KIII $\beta$  antagonist IN-9 was reversed by conditioned medium from untreated cells (Fig. 6, F and G), warranting studies to identify prosurvival factors in the conditioned medium samples. Liquid chromatography-mass spectrometry analysis on conditioned medium

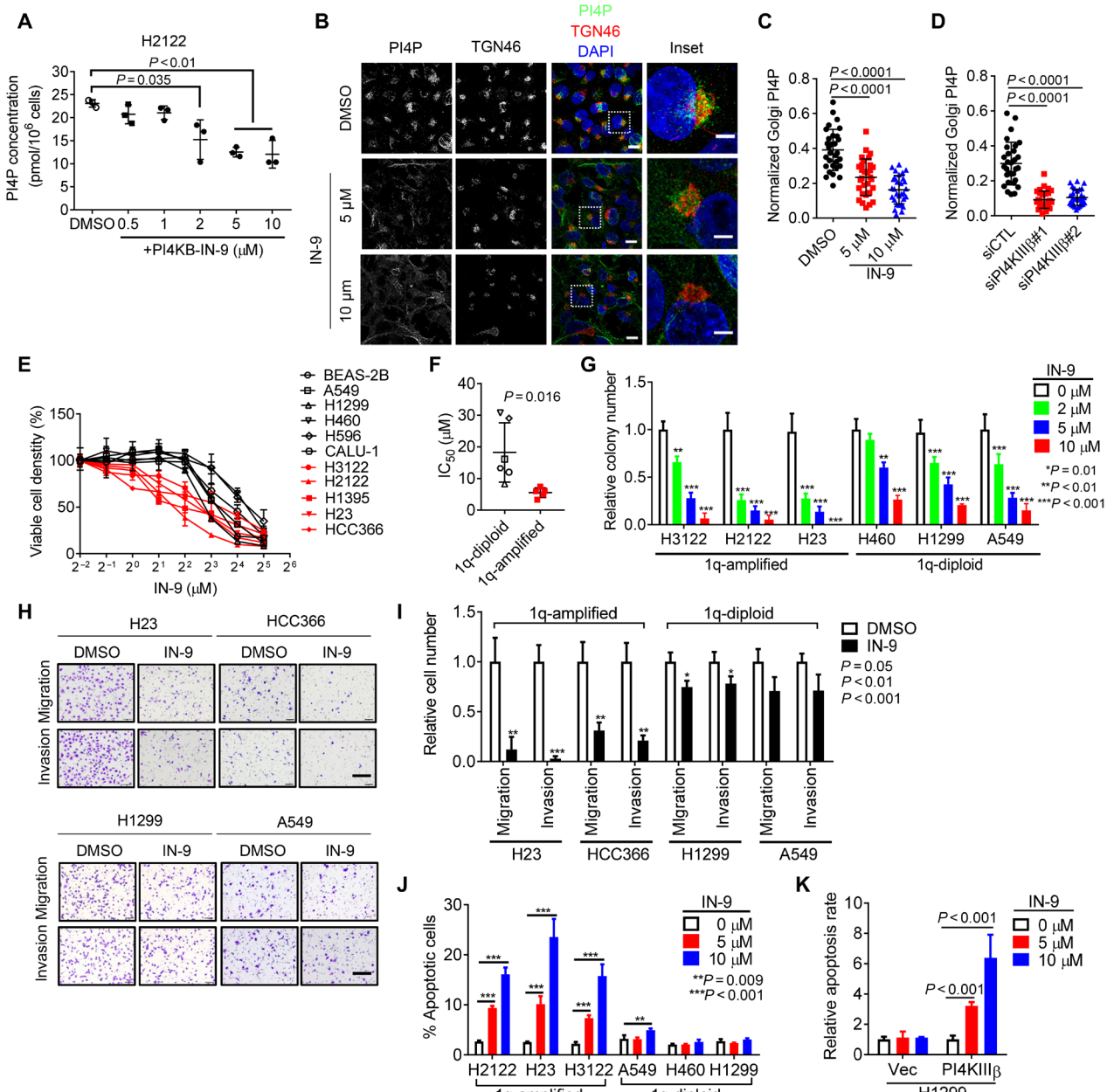


**Fig. 3. PI4KIIIβ is an actionable target in 1q-amplified lung cancer cells.** (A) Total cellular PI4P concentrations in H2122 cells treated for 24 hours with different concentrations of IN-9 or vehicle [dimethyl sulfoxide (DMSO)] determined by ELISA. (B) Single-channel and merged images of staining in H23 cells treated with different concentrations of IN-9 or DMSO for 16 hours. Golgi-resident PI4P was identified by merging PI4P (green) with the trans-Golgi marker TGN46 (red). Boxed regions are illustrated at higher magnification (insets). Scale bars, 15 and 5 μm (insets). (C and D) Golgi-resident PI4P identified as described in (B) in each H23 cell (dot) after treatment with IN-9 (C) or transfection with PI4KIIIβ siRNA (D). (E) Relative densities of 1q-amplified (red) and 1q-diploid (black) human lung adenocarcinoma cell lines determined by WST-1 assays after 4 days of different doses of IN-9 treatment. (F) Half-maximal inhibitory (IC<sub>50</sub>) concentrations of IN-9 determined from (E). (G) Colonies formed on plastic after 7 days of IN-9 treatment. DMSO (0 μM). Results are expressed relative to DMSO control. (H and I) Migrated and invaded cancer cells in Transwell chambers (H) were quantified and plotted (I) after IN-9 treatment for 16 hours. Scale bars, 200 μm. (J and K) Annexin V/propidium iodide flow cytometry to detect apoptotic cells after 24-hour IN-9 treatment of 1q-amplified or 1q-diploid lung cancer cells (J) or H1299 cells that ectopically express PI4KIIIβ or empty vector (K).

samples identified approximately 500 proteins ( $\geq 2$  peptides per protein, 1% false discovery rate), 33 of which decreased after PI4KIIIβ depletion in both H23 and H2122 cells (fold change,  $>1.4$ ), including proteins reported to exert prosurvival and/or prometastatic activities, such as semaphorin-3C (SEMA3C), lysyl hydroxylase-3 (PLOD3), tissue inhibitor of metalloproteinase-1 (TIMP1), peroxiredoxin-5 (PRDX5),

annexin-A2 (ANXA2), clusterin (CLU), and stanniocalcin-2 (STC2) (Fig. 6H and table S2) (40–46). Western blot analysis of conditioned medium samples confirmed that five of these proteins (CLU, PLOD3, TIMP1, SEMA3C, and STC2) were reduced by short hairpin RNA (shRNA)-mediated PI4KIIIβ depletion (Fig. 6I and fig. S9A). These reductions were not due to decreased protein synthesis, as their

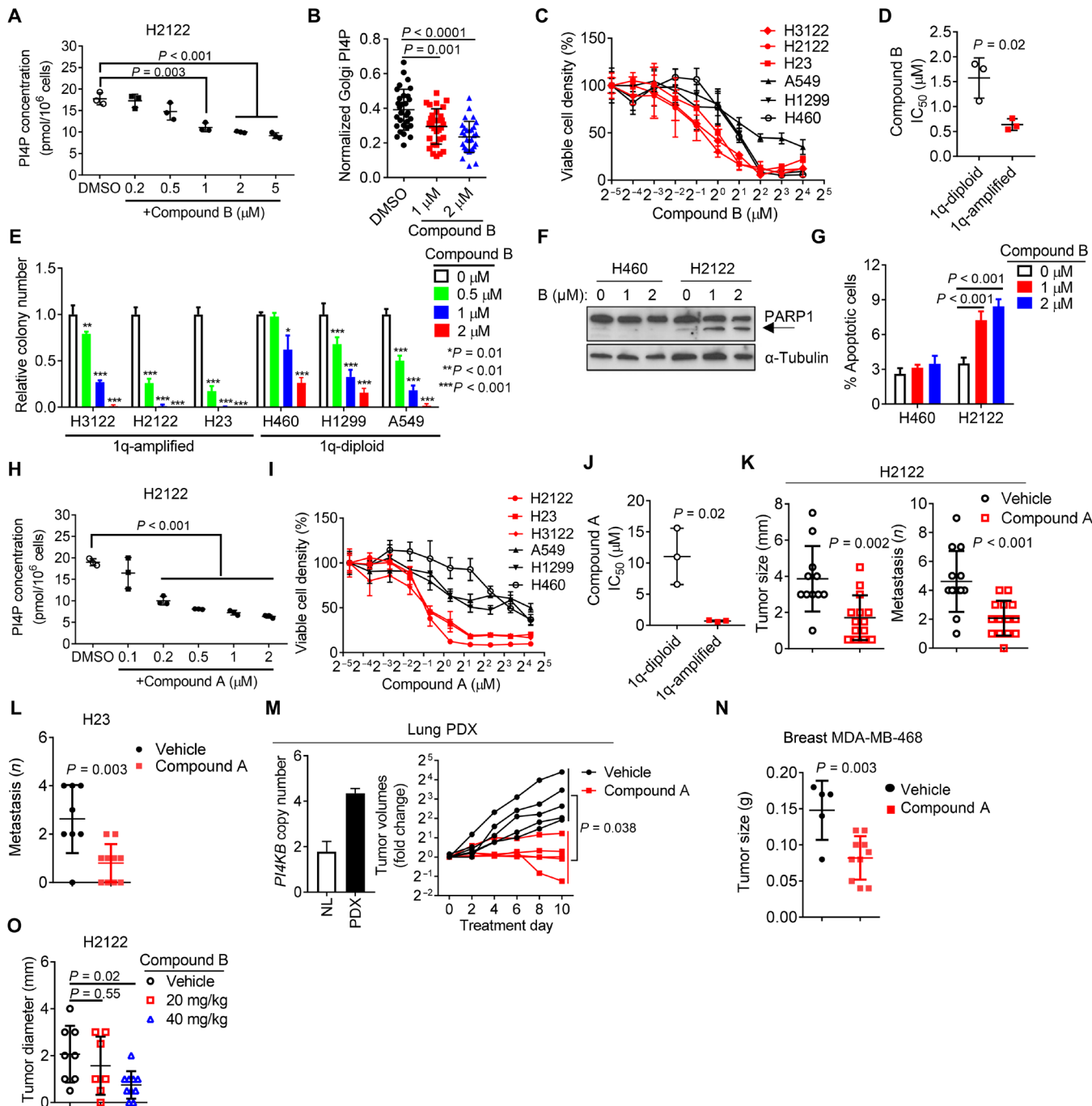


**Fig. 4. PI4KIIIβ is an actionable target in 1q-amplified cancers.** (A) Total cellular PI4P concentrations in H2122 cells after 24-hour treatment with compound B or vehicle DMSO determined by ELISA. Each dot is a replicate sample. (B) Golgi-resident PI4P in each H2122 cell (dot) determined by immunofluorescence staining as described in Fig. 3B. Cells treated for 16 hours with compound B or DMSO. (C) Relative densities of 1q-amplified (red) and 1q-diploid (black) human lung adenocarcinoma cell lines determined after 4 days of compound B treatment. (D) IC<sub>50</sub> concentrations determined on the basis of (C). (E) Colonies formed on plastic after 7 days of compound B treatment. Results expressed relative to DMSO control (0  $\mu\text{M}$ ). (F and G) Western blot analysis to detect apoptotic cells on the basis of PARP1 [poly(adenosine diphosphate–ribose) polymerase 1] cleavage (arrow) (F) and annexin V/propidium iodide flow cytometry (G) in 1q-amplified (H2122) and 1q-diploid (H460) lung cancer cells treated for 24 hours with compound B. (H) Total cellular PI4P in H2122 cells treated with different doses of compound B determined by ELISA. (I) Relative densities of 1q-amplified (red) and 1q-diploid (black) lung cancer cells determined after 4 days of compound A treatment. (J) IC<sub>50</sub> concentrations determined on the basis of (I). (K) H2122 orthotopic lung tumor diameters (left) and metastases (right) after 7 days of compound A treatment. (L) Metastases generated by H23 orthotopic lung tumors after 7 days of compound A treatment. (M) PCR detection of PI4KB copy numbers in a lung adenocarcinoma patient-derived xenograft (PDX) (left). PDX tumor volumes in mice treated with compound A are expressed as fold change relative to time ( $t = 0$ ) (right). (N) MDA-MB-468 mammary tumor weights after 7 days of compound A treatment. (O) H2122 orthotopic lung tumor diameters after 21 days of compound B treatment at indicated doses.

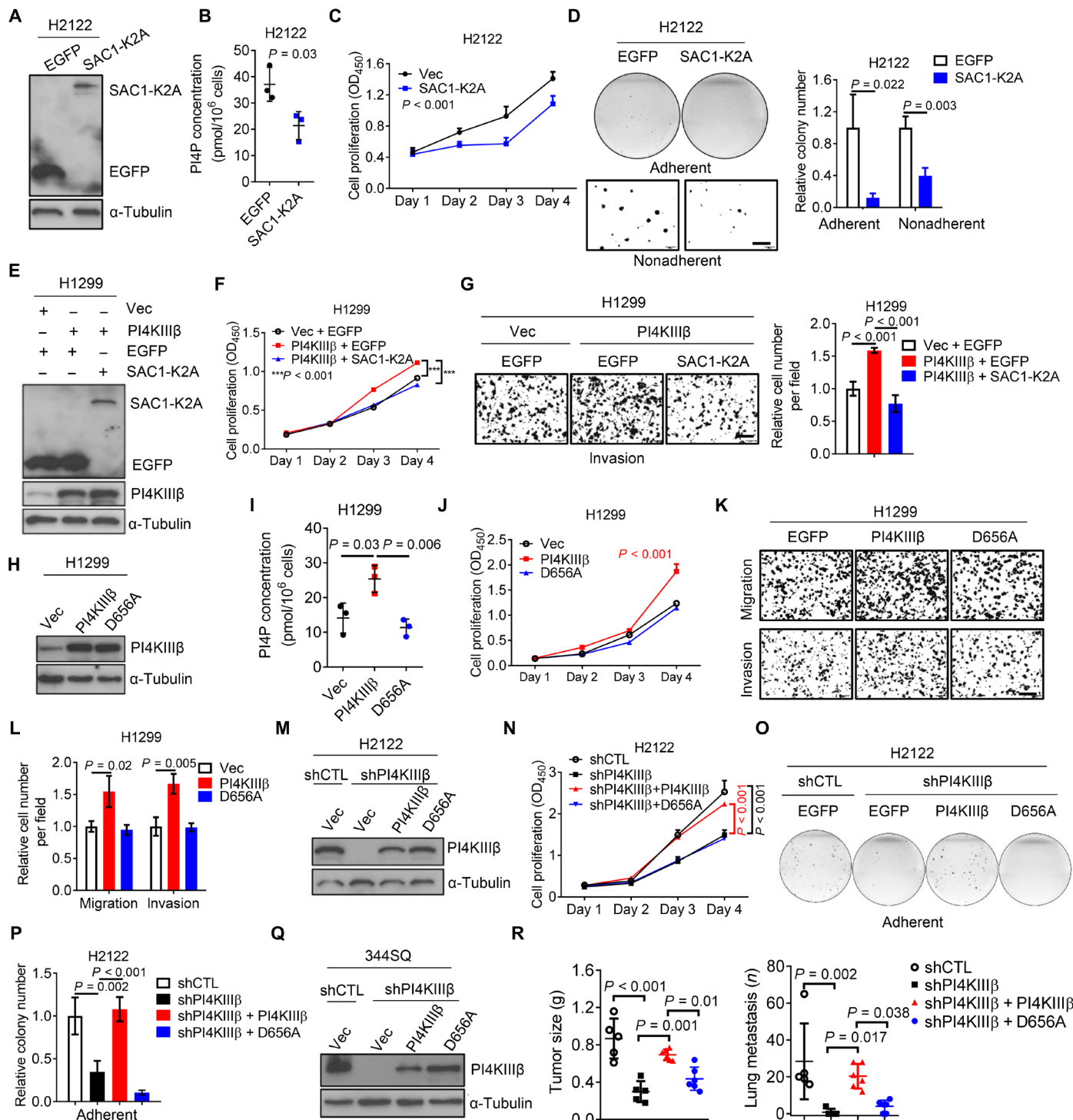


**Fig. 5. PI4KIII $\beta$ -dependent kinase activity promotes tumor growth and metastasis.** (A) Western blot analysis of ectopic SAC1-K2A expression in H2122 cells. (B) Total cellular PI4P concentrations in H2122 cells transfected with SAC1-K2A or EGFP (enhanced green fluorescent protein) determined by ELISA. (C) Cell proliferation determined by WST-1 assays. (D) Colonies formed on six-well plates (adherent) and in soft agar (nonadherent). Scale bar, 200  $\mu$ m. (E) Western blot analysis of ectopic PI4KIII $\beta$  and SAC1-K2A expression. (F) Cell proliferation determined by WST-1 assays. (G) Invaded cells in Transwell chambers. Scale bar, 200  $\mu$ m. (H) Western blot analysis of ectopic wild-type or kinase-dead mutant PI4KIII $\beta$  (D656A) in H1299 cells. (I) Total cellular PI4P concentrations in cells generated in (H) determined by ELISA. (J) Cell proliferation determined by WST-1 assays. (K) Migrated and invaded cells in Transwell chambers. Scale bar, 200  $\mu$ m. (L) Quantification of cells in (K). (M) Western blot analysis of ectopic wild-type or kinase-dead mutant (D656A) PI4KIII $\beta$  expression in H2122\_shPI4KIII $\beta$  cells. (N) Cell proliferation determined by WST-1 assays. (O) Colonies formed on plastic. (P) Quantification of colonies in (O). (Q) Western blot analysis of ectopic wild-type or kinase-dead mutant (D656A) PI4KIII $\beta$  expression in 344SQ\_shPI4KIII $\beta$  cells. (R) Flank tumor weights (left) and lung metastasis numbers (right) in syngeneic, immunocompetent mice. OD<sub>450</sub>, optical density at 450 nm.

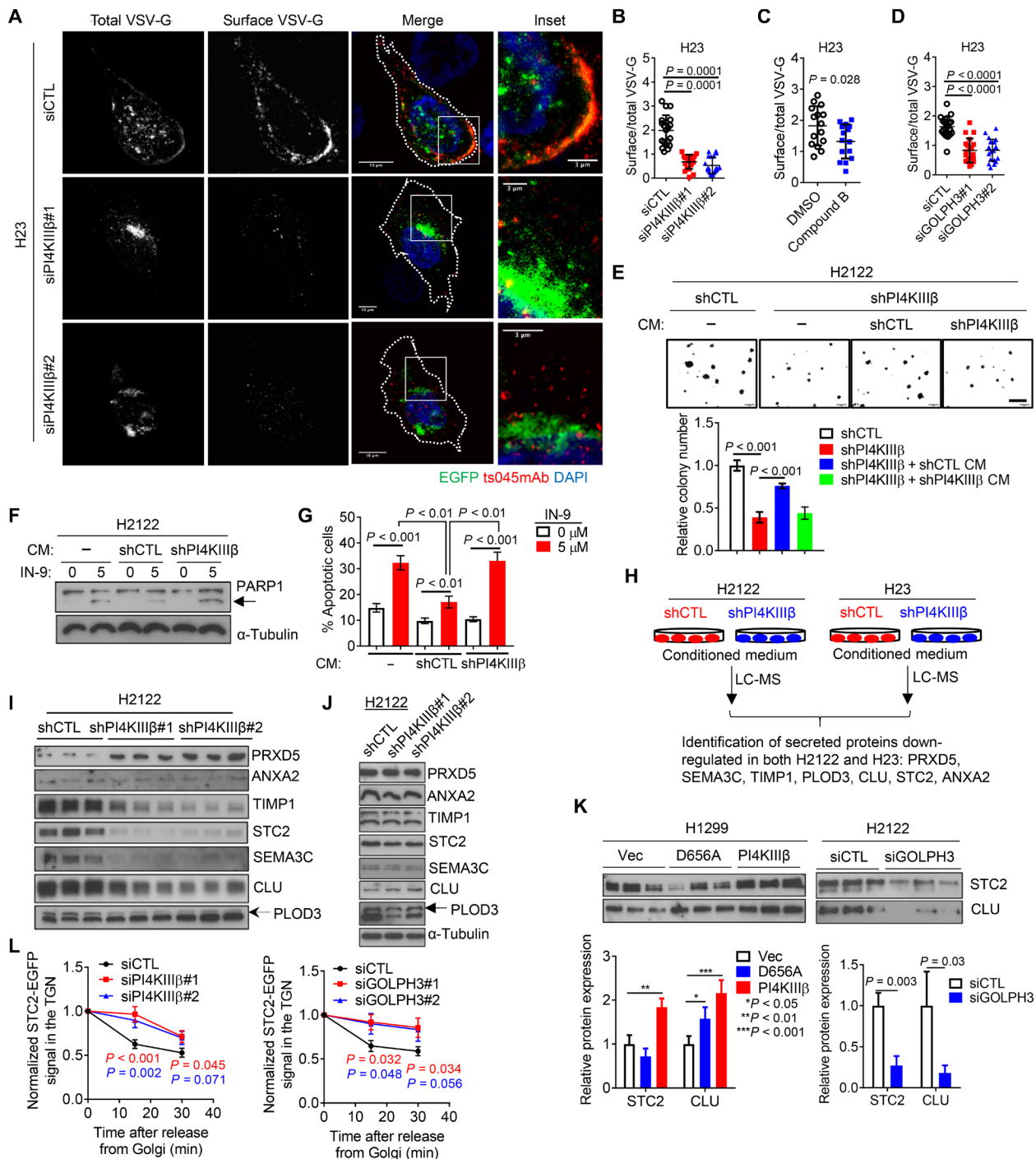


**Fig. 6. PI4KIII $\beta$  drives secretion of prometastatic proteins.** (A) Single-channel and merged images of plasma membrane–associated VSV-G (red) and total VSV-G (green) in H23 cells transfected with indicated siRNAs. Boxed areas in merged images are magnified (insets). Scale bars, 10 and 3  $\mu$ m (insets). (B to D) Surface VSV-G to total VSV-G in H23 cells transfected with siPi4KIII $\beta$  (B), treated with compound B (C), or transfected with siGOLPH3 (D) ( $n > 15$  cells per group). (E) Nonadherent colonies formed by shPi4KIII $\beta$ - and shCTL-transfected H2122 cells treated with conditioned medium (CM) from shCTL- or shPi4KIII $\beta$ -transfected H2122 cells were imaged and quantified. Fresh medium (–) was included as a control. Scale bar, 200  $\mu$ m. (F) Western blot analysis to detect PARP1 cleavage (arrow) in apoptotic cells. (G) Annexin V/propidium iodide flow cytometric detection of apoptotic shRNA-transfected H2122 cells after treatment with PI4KIII $\beta$  antagonist IN-9 or vehicle (0  $\mu$ M). (H) Schema of liquid chromatography–mass spectrometry (LC-MS) analysis of conditioned medium samples from H23 and H2122 cells. Identified proteins of interest are listed. (I and J) Western blot analysis of conditioned medium samples (I) and cell lysates (J). Specific PLOD3 band is indicated (arrow). (K) Western blot analysis of conditioned medium samples isolated from cells stably transfected with indicated vectors was performed to quantify STC2 and CLU proteins. The relative protein amounts were quantified in ImageJ (bar graph). (L) Quantification of Golgi-localized STC2 relative to  $t = 0$  ( $n = 20$  cells per time point) from vesicular release assays on H23 cells cotransfected with GFP-tagged STC2 and indicated siRNAs. Results are from images taken before ( $t = 0$ ) and 15 and 30 min after switching to a temperature that permits Golgi release. Images are in fig. S9 (D and E).

amounts were not reduced in total lysates of PI4KIII $\beta$ -deficient cells (Fig. 6J). Conversely, their secretion was enhanced by ectopic expression of wild-type but not kinase-dead mutant PI4KIII $\beta$  in H1299 cells and was reduced by siRNA-mediated GOLPH3 depletion in H2122 cells (Fig. 6K and fig. S9, B and C). In 1q-amplified H23 cells, release of STC2-containing vesicles from the Golgi was PI4KIII $\beta$  and GOLPH3 dependent (Fig. 6L and fig. S9, D and E). PI4KIII $\beta$ -dependent protein secretion was higher and more sharply inhibited by IN-9 treatment in 1q-amplified than in 1q-diploid lung cancer cells (fig. S10, A to D). These findings identify a PI4KIII $\beta$ -dependent secretome in 1q-amplified lung cancer cells.

Our model thus predicts that CLU, SEMA3C, PLOD3, TIMP1, and STC2 are prosurvival and prometastatic effectors of PI4KIII $\beta$ . To address this possibility, we first examined their expression in the TCGA lung adenocarcinoma cohort, which showed that high expression of a signature composed of these five genes was associated with shorter survival (Fig. 7A). Next, we performed siRNA-mediated depletion studies on these five genes and found that 1q-amplified and 1q-diploid lung cancer cells required these proteins to varying degrees for colony formation, migration, and invasion, but only 1q-amplified cells required PLOD3 and TIMP1 for survival (Fig. 7, B to J, and fig. S11, A to F). Depletion of PLOD3 or TIMP1 increased apoptosis more prominently in ectopic PI4KIII $\beta$ -expressing H1299 cells than in control transfectants (fig. S11G), demonstrating a causal relationship between heightened PI4KIII $\beta$  expression and addiction to secreted factors. All five genes were essential for the growth and metastatic activity of orthotopic lung tumors generated by H2122 cells (Fig. 7, K and L). Depletion of these factors induced apoptosis in KRAS-mutant (H2122) and wild-type (H3122) 1q-amplified cells (Fig. 7, I and J, and fig. S11H), arguing against synthetic interactions with mutant KRAS.

PLOD3 has lysyl hydroxylase (LH) and glycosyltransferase (GLT) domains that modify collagen molecules (46). To investigate the way in which PLOD3 maintains tumor cell survival, we reconstituted PLOD3-deficient H2122 cells with wild-type or mutant PLOD3 that lacks either LH or GLT activities. Unexpectedly, H2122 cells were rescued from siPLOD3-induced apoptosis by either wild-type or mutant PLOD3 (fig. S11I), suggesting that PLOD3 promotes cell survival through a noncatalytic mechanism. Because PLOD3 is reported to form a complex with MMP9 on the cell surface (47), we speculated that MMP9 is a prosurvival mediator of PLOD3. siRNA-mediated MMP9 depletion induced apoptosis in H2122 cells (fig. S11J), and apoptosis was reversed by the addition of recombinant PLOD3 protein to the medium of PLOD3-deficient H2122 cells but not H2122 cells that are deficient in PLOD3 and MMP9 (fig. S11K). Our finding that MMP9 and TIMP1 have similar functions is paradoxical given that TIMP1 inhibits MMP9 (48). To address this paradox, we quantified MMP9 activity in conditioned medium samples from H2122 cells and found that MMP activity was reduced by siRNA-mediated depletion of PLOD3 but not altered by depletion of TIMP1 (fig. S11L), suggesting that TIMP1 does not inhibit PLOD3-dependent MMP9 activity in H2122 cells.

### PI4KIII $\beta$ -dependent secretion regulates the tumor microenvironment

To determine whether PI4KIII $\beta$  drives the secretion of cytokines that play key roles in the tumor microenvironment, we subjected conditioned medium samples from H2122 cells and 344SQ cells to multiplexed cytokine assays and found that, among the cytokines present at concentrations of at least 1 pg/ml, many were reduced 5- to 10-fold by PI4KIII $\beta$  depletion, including G-CSF, GM-CSF,

Fractalkine, LIX, CXCL1, IL-8, IL-1 $\alpha$ , VEGF, MIP-1 $\alpha$ , and MIP-2 (Fig. 8A and fig. S12A). To characterize the contributions of PI4KIII $\beta$ -dependent cytokines to processes in the tumor microenvironment, we quantified immune cell populations in 344SQ flank tumors generated in syngeneic, immunocompetent mice and found that CD11b $^+$ GR1 $^+$  myeloid-derived suppressor cells (MDSCs) were fewer in PI4KIII $\beta$ -deficient than in PI4KIII $\beta$ -replete tumors (Fig. 8B), whereas CD4 $^+$  and CD8 $^+$  T cell subsets, dendritic cells, granulocytes, and macrophages were not different (fig. S12, B to E). Similar numbers of MDSCs were generated in splenocytes cocultured with PI4KIII $\beta$ -deficient or PI4KIII $\beta$ -replete 344SQ cells (fig. S12F), suggesting that PI4KIII $\beta$ -driven secretion does not govern MDSC differentiation. Although microvessel density in PI4KIII $\beta$ -deficient and PI4KIII $\beta$ -replete 344SQ tumors was not different (Fig. 8C), human umbilical vein endothelial cells (HUVECs) exhibited reduced chemotaxis and generated fewer tubes in coculture with PI4KIII $\beta$ -deficient than PI4KIII $\beta$ -replete H2122 cells (Fig. 8, D and E), suggesting that PI4KIII $\beta$ -dependent secreted factors that promote angiogenesis in HUVEC assays are nonessential for angiogenesis in 344SQ tumors. Furthermore,  $\alpha$ -smooth muscle actin $^+$  cancer-associated fibroblasts (CAFs) were fewer in PI4KIII $\beta$ -deficient than in PI4KIII $\beta$ -replete 344SQ tumors (Fig. 8F), exhibited reduced migratory activity toward PI4KIII $\beta$ -deficient than PI4KIII $\beta$ -replete 344SQ cells (Fig. 8G), and enhanced the total number of invasive projections emanating from multicellular aggregates containing PI4KIII $\beta$ -replete but not PI4KIII $\beta$ -deficient 344SQ cells (Fig. 8H). The reduced invasiveness was due, in part, to a loss of “leader-follower cell” structures containing a CAF at the tip and tumor cells that collectively follow behind (Fig. 8, I and J) (49). These findings suggest that PI4KIII $\beta$ -dependent secretion plays a broad regulatory role in the tumor microenvironment.

### DISCUSSION

Although epithelial cancers secrete a variety of effector proteins that play key roles in tumor progression, inhibitors of MMPs and other secreted effectors in the tumor microenvironment have been largely ineffective in clinical trials (3). A better understanding of the way in which malignant secretion is activated in cancer may lead to improved therapeutic approaches (5). Here, we show that 1q amplifications activate malignant secretion and underlie an actionable vulnerability owing to an apparent “addiction” to secreted factors (Fig. 8K). We further show that secretory blockade has the potential to suppress not only survival signals but also paracrine factors that drive prometastatic processes in the tumor microenvironment. The clinical implications of secretory blockade could be substantial based on the various tumor types that harbor 1q amplifications and the broad range of inflammatory, fibrotic, and senescence-related diseases that are driven by heightened secretion.

Phosphorylated PIs increase as a consequence of cancer-associated somatic mutations and play a crucial role in tumor progression by serving as membrane-docking sites for proteins that drive tumor growth and metastasis. Examples include diphosphorylated PI-4,5-P2 and triphosphorylated PI-3,4,5-P3, which are elevated as a consequence of somatic mutations in the type 2 PIP kinases, PI-3-kinases, and/or PTEN lipid phosphatase (50, 51). Here, we show that total cellular PI4P concentrations are elevated due to *PI4KB* gene amplifications. PI4P is generated by four mammalian PI4K enzymes, including two type II kinases (*PI4KII $\alpha$*  and *PI4KII $\beta$* ) and two type III kinases

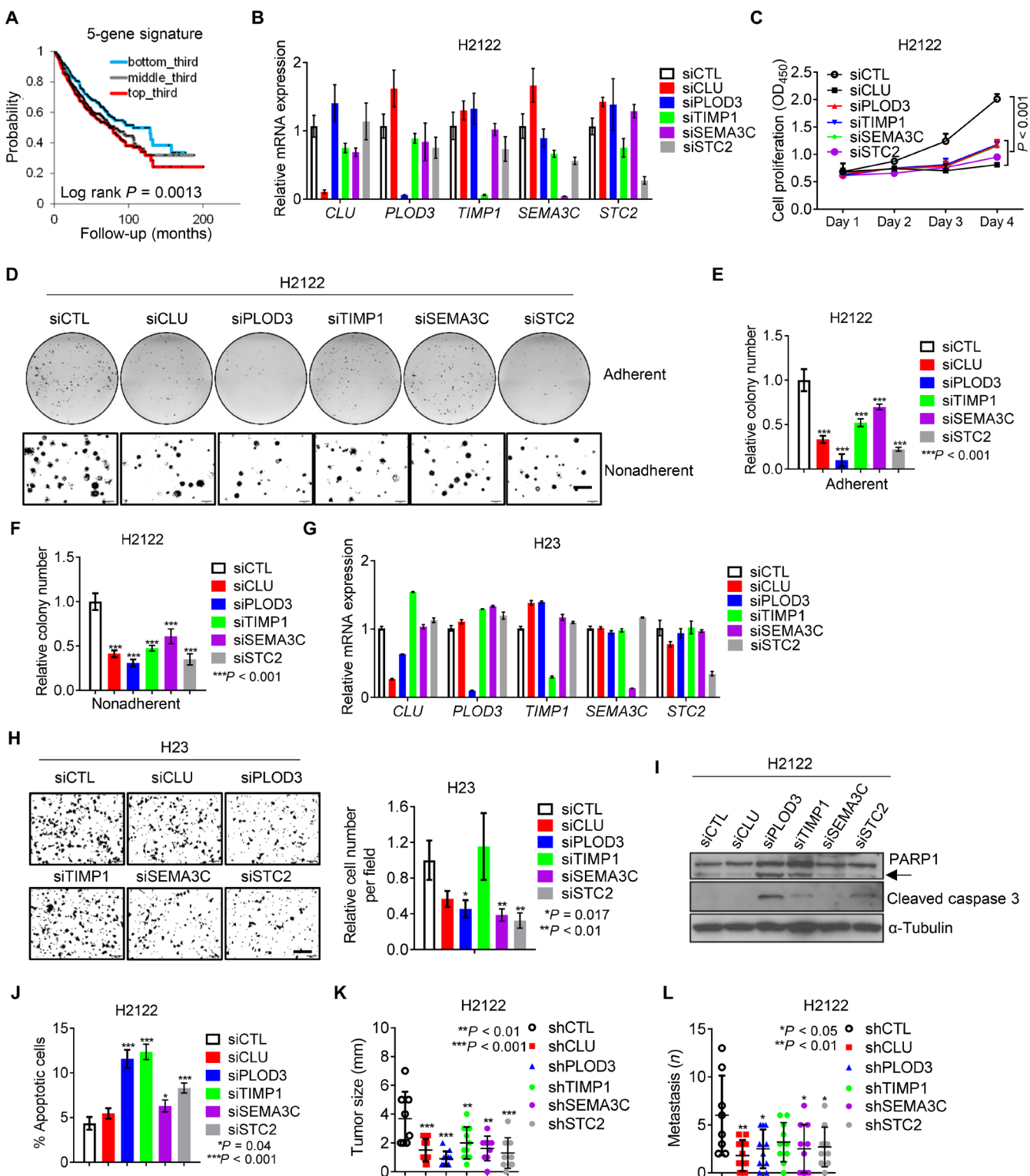


**Fig. 7. PI4KIII $\beta$ -dependent secreted proteins promote metastasis.** (A) Kaplan-Meier plot of TCGA lung adenocarcinomas with low (bottom-third), intermediate (middle-third), or high (top-third) expression of a five-gene signature (*SEMA3C*, *TIMP1*, *STC2*, *PLOD3*, and *CLU*). (B) Quantitative PCR analysis of mRNA expression in H2122 cells transfected with the indicated siRNAs. (C) Cell proliferation determined by WST-1 assays. (D) Colonies formed by siRNA-transfected H2122 cells on plastic and in soft agar. Scale bar, 200  $\mu$ m. (E and F) Quantification of colonies on plastic (E) and in soft agar (F) as shown in (D). (G) Quantitative PCR analysis of mRNA expression in H2122 cells transfected with the indicated siRNAs. (H) Colonies formed in soft agar were imaged and quantified. Scale bar, 200  $\mu$ m. (I) Western blot analysis to detect cleavage of PARP1 (arrow) and caspase 3 in apoptotic cells. (J) Annexin V/propidium iodide flow cytometric detection of apoptotic H2122 cells. (K and L) H2122 orthotopic tumor diameters (K) and metastasis numbers (L) per mouse.

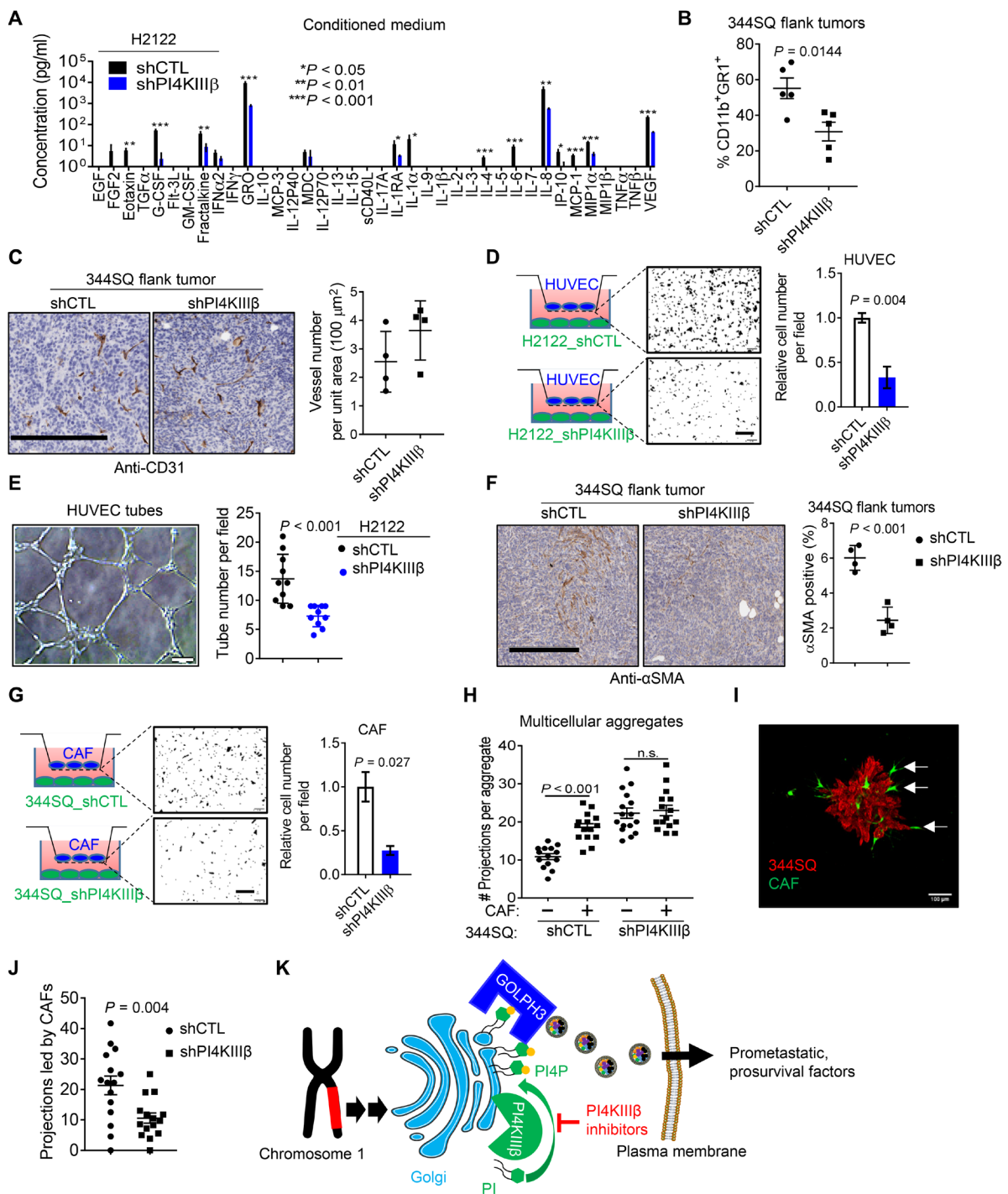


**Fig. 8. PI4KIII $\beta$ -dependent secretion regulates processes in the tumor microenvironment.** (A) Concentrations of secreted factors in conditioned medium samples. (B) MDSCs (CD11b $^+$ GR1 $^+$ ) in 344SQ flank tumors expressed as percentage of total CD45 $^+$  cells. (C) CD31 $^+$  cells in flank tumors generated by injection of 344SQ cells into syngeneic, immunocompetent mice. Scale bar, 300  $\mu$ m. Microvessel density quantification in each cohort (plot). (D) Migrated human umbilical vein endothelial cells (HUVECs) in coculture with H2122 cells in Transwell chambers. Scale bar, 200  $\mu$ m. (E) HUVEC tubes formed in coculture with H2122 cells. Scale bar, 100  $\mu$ m. Quantification of HUVEC tubes per field. (F)  $\alpha$ -Smooth muscle actin-positive ( $\alpha$ SMA $^+$ ) cells in flank tumors generated by injection of 344SQ cells into syngeneic, immunocompetent mice. Scale bar, 300  $\mu$ m. Quantification of  $\alpha$ SMA $^+$  cells in each cohort (plot). (G) Migrated cancer-associated fibroblasts (CAFs) in coculture with 344SQ cells in Transwell chambers. Scale bar, 200  $\mu$ m. (H) Numbers of invasive projections per multicellular aggregate. Aggregates containing RFP-tagged 344SQ cells alone (–) or 344SQ cells and GFP-tagged CAFs (+) were seeded in collagen gels and imaged. n.s., not significant. (I) Multicellular aggregate with leader-follower cell structures containing a CAF at the tip and collectively invasive 344SQ cells that follow behind (arrows). Scale bar, 100  $\mu$ m. (J) Numbers of leader-follower cell structures per aggregate in (I). (K) Schematic illustration of the proposed model. The 1q amplicon encodes PI4KIII $\beta$ , which activates PI4P synthesis, leading to GOLPH3 recruitment, increased anterograde vesicular trafficking, and enhanced secretion of prosurvival and prometastatic factors. Secretion can be blocked by PI4KIII $\beta$  antagonists.

(PI4KIII $\alpha$  and PI4KIII $\beta$ ), that reside in distinct subcellular compartments (9). The Golgi pool of PI4P is increased by PI4KIII $\beta$  and PI4KII $\alpha$  and reduced by the SAC-1 PI4P phosphatase (9). The genes encoding PI4KII $\alpha$  and SAC-1 are rarely mutated in cancer, but high PI4KII $\alpha$  expression has been shown to be protumorigenic (52). Thus, the Golgi pool of PI4P plays a crucial role in cancer development.

Heightened secretion of prometastatic effector proteins results from genetic amplification of the PI4P-binding proteins GOLPH3 and PITPNM1 (7, 8). Here, we show that *PI4KB* is coamplified with *GOLPH3* and *PITPNM1*, corroborating the vital role that PI4P plays as a Golgi membrane insertion site for GOLPH3 and PITPNM1 (8, 53). Furthermore, we show that *PI4KB* genetic amplifications drive tumor progression by increasing the secretion of prosurvival and prometastatic effector proteins, including TIMP1, SEMA3C, CLU, PLOD3, and STC2. We also show that PI4KIII $\beta$ -dependent vesicular trafficking is sustained by coamplified Golgi-resident proteins that anchor PI4KIII $\beta$  to Golgi membranes and acidify Golgi lumens and that this functional circuitry can be disrupted by treatment with small-molecule PI4KIII $\beta$  antagonists that preferentially impair the survival of 1q-amplified cancer cells. Our findings support a model in which chromosome 1q amplifications create a dependency on PI4KIII $\beta$ -dependent secretion for survival. The cell-intrinsic and cell-extrinsic mechanisms through which oncogene addiction occurs (54) are similar to those ascribed to the PI4KIII $\beta$ -dependent effector proteins identified here (43, 46, 55–57).

However, there are limitations to our study. Ectopic PI4KIII $\beta$  expression in 1q-diploid cancer cells does not recapitulate the full consequences of a 1q amplicon that contains PI4KIII $\beta$  and multiple other regulators of Golgi and vesicular trafficking functions. The total cellular PI4P and Golgi-resident PI4P assays used in this study do not provide robust assessments of Golgi-resident PI4P concentrations and therefore do not optimally gauge the effect of pharmacologic PI4KIII $\beta$  antagonism on the Golgi. Our short-term treatment studies did not evaluate therapeutic response durability or acquired resistance to PI4KIII $\beta$  antagonism in 1q-amplified cancer cells. Although the mice treated with PI4KIII $\beta$  antagonists demonstrated no overt signs of toxicity, we did not perform an in-depth toxicity analysis.

In conclusion, we have identified an actionable secretory vulnerability in cancers harboring chromosome 1q amplifications that are associated with a worse prognosis. Our findings provide a foundation for therapeutic strategies designed to target the secretory process in cancer cells. In support of this concept, photodynamic therapies that inhibit Golgi-dependent protein secretion have antitumor efficacy (58). The prevalence of 1q amplifications across multiple tumor types, the biological relevance of a 1q-encoded functional circuitry that drives tumor growth and metastasis, the availability of digital droplet PCR assays to identify patients with 1q-amplified tumors, and the efficacy of small-molecule PI4KIII $\beta$  antagonists highlight the clinical relevance of 1q amplifications in cancer. PI4KIII $\beta$  antagonists that are under development for non-oncologic indications can be repurposed for “basket” clinical trials to test their efficacy in cancer patients carrying 1q amplifications.

## MATERIALS AND METHODS

### Study design

The objectives of our study were to elucidate mechanisms by which the conventional secretory pathway is activated in cancer and to identify therapeutic vulnerabilities in cancer cells that rely on secre-

tion for survival and metastasis. The components of our study include publicly available human tumor databases, in vivo and in vitro models of metastatic cancers, cellular and biochemical assays of conventional secretory pathway activity, small-molecule inhibitors of PI4KIII $\beta$ , biochemical and cellular assays of PI4KIII $\beta$  inhibitor activity, and mass spectrometric analysis of conditioned medium samples. Observations made in human tumor databases provided a rationale for studies on PI4KIII $\beta$  in 1q-amplified cancer cell lines and mice bearing 1q-amplified cancers, including assays of PI4KIII $\beta$  activity and the effect of pharmacologic and genetic PI4KIII $\beta$  inhibition on cancer cell viability, tumor size, and metastatic activity. Tumor-bearing mice were randomized to treatment cohorts. Investigators were not blinded to sample identities during analysis. Cohort sample sizes were calculated to have 80% power to detect a twofold change in tumor size between groups, using a two-group *t* test with a two-sided type I error rate of 0.05. Each experiment involved biological replicate samples (at least triplicate). With the exception of the autochthonous tumor studies, each experiment was repeated at least once.

### Animal husbandry

All mouse studies were approved by the Institutional Animal Care and Use Committee at The University of Texas MD Anderson Cancer Center. K-ras<sup>LSL-G12D</sup> mice were purchased from The Jackson Laboratory. The 129/SV syngeneic mice and nu/nu mice were bred in-house. Mice received standard care and were euthanized according to the standards set forth by the Institutional Animal Care and Use Committee. To generate autochthonous lung tumors, 50,000 GFP-Cre or *PI4KB*-cre lentivirus particles were delivered into the lungs of K-ras<sup>LSL-G12D</sup> mice through an endotracheal tube as reported previously (34). As we have described (59), KP cells were injected subcutaneously ( $10^6$  cells) or intravenously ( $10^5$  cells) into syngeneic, immunocompetent mice, and human lung cancer cells were injected intrathoracically ( $10^6$  cells) into nu/nu mice. Mice bearing human H2122 or H23 orthotopic lung tumors were treated with compound A (100 mg/kg) or vehicle [5% dimethyl sulfoxide (DMSO), 20% hydroxypropyl beta cyclodextrin (HPBCD), 2% polysorbate 80, and 10% PEG300 (polyethylene glycol 300)] twice daily by intraperitoneal injection beginning 21 days after tumor cell injection and continued for 7 days. Nu/nu mice bearing human MB-MDA-468 breast tumors or lung cancer patient-derived xenografts were treated for 7 days with vehicle or compound A once tumors reached 100 mm<sup>3</sup>. Nu/nu mice bearing human H2122 orthotopic lung tumors were treated subcutaneously with compound B [20 or 40 mg/kg plus ritonavir (20 mg/kg)] or vehicle (5% DMSO, 20% HPBCD, 2% Poly 80, and 10% PEG300) twice daily beginning 7 days after tumor cell injection and continued for 21 days. For each model, necropsies were performed to quantify primary tumor size and metastatic tumor burden.

### Micro-CT

As previously reported (60), the mice were placed in an inhalation anesthesia induction chamber (isoflurane, 5% for induction and 1.5 to 3% for maintenance). When the mice were fully anesthetized, an endotracheal tube (22 gauge  $\times$  1 inch length) was placed using a BioLite mouse intubation system (Braintree Scientific). The mice were then placed onto a holder and moved to a CT scanner (XRAD 225Cx, Precision XRay Incorporated). The CT parameters used were 60 kV, 4 mA, and 3 rpm, and the subsequent image resolution was 100  $\mu$ m. The mice were mechanically ventilated at 60 breaths/min

throughout the procedure, and a 20-s breath hold was applied during the acquisition at 20 cm/H<sub>2</sub>O. The pressure was monitored for consistency through an inline manometer. After processing images (ImageJ), tumor nodule areas were calculated from the major radius (*a*) and minor radius (*b*) of each nodule using the formula of an ellipse (area =  $\pi \times a \times b$ ).

### Human studies

Human tumor specimens were obtained through an institutional review board (IRB)-approved protocol and with informed consent, and the analysis of the human tissue specimens was approved by an IRB at MD Anderson Cancer Center. Digital droplet PCR and quantitative reverse transcription PCR assays were performed on a preexisting tissue bank of early-stage lung adenocarcinomas isolated surgically from patients that had been annotated on the basis of molecular and clinical parameters (table S1). For analysis of mRNA expression and lung cancer patient survival, we examined a compendium dataset of 11 published expression profiling datasets for human lung adenocarcinomas (61–65); patients represented in both Shedd and Chitale datasets were removed from the Shedd dataset, patients represented in both the Sato and Tang datasets were removed from the Tang dataset, and one patient from Bild dataset thought to potentially represent squamous cell carcinoma was also removed, leaving *n* = 1453 tumors in total; patient survival was capped at 200 months. To analyze the prognostic value of a given gene signature, the average of the *z*-normalized values for the genes was evaluated across the lung compendium cohort. The Kaplan-Meier method with log-rank test was used to evaluate overall survival curves for mouse cohorts and patients. Plots were generated for the respective groups using GraphPad Prism version 7.0 or WinSTAT ([www.winstat.com](http://www.winstat.com)). For the pan-cancer analysis, we collected data from TCGA (66, 67). For determining copy number alterations in TCGA data, GISTIC 2.0 was applied to the transformed copy number data obtained from Affymetrix SNP 6.0 arrays [*n* = 10,845 tumor profiles in all, 516 from lung adenocarcinoma or TCGA LUAD (lung adenocarcinoma) project], with a noise threshold used to determine copy gain or loss; low-level gene gain, high-level gene amplification, low-level copy loss, or high-level copy loss was inferred using the “thresholded” calls as made by Broad Firehose pipeline (using +1, +2, -1, or -2, respectively) (68).

### Statistical analysis

Unless stated otherwise, the results shown are representative of replicated experiments and are the means  $\pm$  SDs from triplicate samples or randomly chosen cells within a field. Statistical evaluations were carried out with Prism 6 (GraphPad Software Inc.). Unpaired two-tailed Student’s *t* tests were used to compare the mean values of two groups. Analysis of variance (ANOVA) with Dunnett’s test was used for comparing multiple treatments to a control. *P* < 0.05 was considered statistically significant. Original data are provided in data file S1.

### SUPPLEMENTARY MATERIALS

[stm.science.org/cgi/content/full/12/527/eaax3772/DC1](https://stm.sciencemag.org/cgi/content/full/12/527/eaax3772/DC1)

#### Materials and Methods

Fig. S1. Chromosome 1q is amplified in a subset of human lung cancer cell lines.

Fig. S2. High expression of Golgi-related genes enhances the metastatic properties of 1q-amplified lung cancer cells.

Fig. S3. 1q-amplified cancers are PI4KIII $\beta$  dependent.

Fig. S4. PI4KB functions cooperatively with coamplified genes on chromosome 1q.

Fig. S5. IN-9 induces apoptosis in 1q-amplified, but not 1q-diploid, lung cancer cells.

Fig. S6. Selective PI4KIII $\beta$  antagonists have activity against 1q-amplified lung cancer cells.

Fig. S7. PI4KIII $\beta$ -dependent PI4P synthesis drives prometastatic properties of 1q-amplified lung cancer cells.

Fig. S8. GOLPH3 mediates prometastatic effects of PI4KIII $\beta$  in 1q-amplified cancer cells.

Fig. S9. GOLPH3 mediates PI4KIII $\beta$ -driven secretion.

Fig. S10. 1q amplification is associated with increased secretion.

Fig. S11. PLOD3 maintains H2122 cell survival by activating MMP9.

Fig. S12. PI4KIII $\beta$ -dependent secretion regulates processes in the tumor microenvironment.

Table S1. Clinical pathological characteristics of lung adenocarcinomas.

Table S2. Liquid chromatography–mass spectrometry of conditioned medium samples.

Table S3. Primers.

Data file S1. Original data.

References (69–79)

[View/request a protocol for this paper from Bio-protocol.](#)

### REFERENCES AND NOTES

- J. L. Paltridge, L. Belle, Y. Khew-Goodall, The secretome in cancer progression. *Biochim. Biophys. Acta* **1834**, 2233–2241 (2013).
- M. Yamauchi, T. H. Barker, D. L. Gibbons, J. M. Kurie, The fibrotic tumor stroma. *J. Clin. Invest.* **128**, 16–25 (2018).
- L. M. Coussens, F. Fingleton, L. M. Matrisian, Matrix metalloproteinase inhibitors and cancer—Trials and tribulations. *Science* **295**, 2387–2392 (2002).
- D. W. McMillin, J. M. Negri, C. S. Mitsiades, The role of tumour-stromal interactions in modifying drug response: Challenges and opportunities. *Nat. Rev. Drug Discov.* **12**, 217–228 (2013).
- J. A. Joyce, J. W. Pollard, Microenvironmental regulation of metastasis. *Nat. Rev. Cancer* **9**, 239–252 (2009).
- F. Zappa, M. Failli, M. A. De Matteis, The Golgi complex in disease and therapy. *Curr. Opin. Cell Biol.* **50**, 102–116 (2018).
- H. C. Dippold, M. M. Ng, S. E. Farber-Katz, S. K. Lee, M. L. Kerr, M. C. Peterman, R. Sim, P. A. Wiharto, K. A. Galbraith, S. Madhavarapu, G. J. Fuchs, T. Meerloo, M. G. Farquhar, H. Zhou, S. J. Field, GOLPH3 bridges phosphatidylinositol-4-phosphate and actomyosin to stretch and shape the Golgi to promote budding. *Cell* **139**, 337–351 (2009).
- N. Halberg, C. A. Sengelaub, K. Navrazhina, H. Molina, K. Uryu, S. F. Tavazoie, PITPNC1 recruits RAB1B to the Golgi network to drive malignant secretion. *Cancer Cell* **29**, 339–353 (2016).
- M. A. De Matteis, C. Wilson, G. D’Angelo, Phosphatidylinositol-4-phosphate: The Golgi and beyond. *Bioessays* **35**, 612–622 (2013).
- K. L. Scott, O. Kabbarah, M. C. Liang, E. Ivanova, V. Anagnostou, J. Wu, S. Dhakal, M. Wu, S. Chen, T. Feinberg, J. Huang, A. Saci, H. R. Widlund, D. E. Fisher, Y. Xiao, D. L. Rimm, A. Protopopov, K. K. Wong, L. Chin, GOLPH3 modulates mTOR signalling and rapamycin sensitivity in cancer. *Nature* **459**, 1085–1090 (2009).
- J. Fan, J. Liu, M. Culley, V. Papadopoulos, Acyl-coenzyme A binding domain containing 3 (ACBD3; PAP7; GCP60): An emerging signaling molecule. *Prog. Lipid Res.* **49**, 218–234 (2010).
- J. Cherfils, Arf GTPases and their effectors: Assembling multivalent membrane-binding platforms. *Curr. Opin. Struct. Biol.* **29**, 67–76 (2014).
- D. C. Bassham, A. A. Sanderfoot, V. Kovaleva, H. Zheng, N. V. Raikhel, AtVPS45 complex formation at the trans-Golgi network. *Mol. Biol. Cell* **11**, 2251–2265 (2000).
- J. Deckstein, J. van Appeldorn, M. Tsangarides, K. Yiannakou, R. Müller, M. Stumpf, S. K. Sukumaran, L. Eichinger, A. A. Noegel, T. Y. Riyahi, The Dictyostelium discoideum GPHR ortholog is an endoplasmic reticulum and Golgi protein with roles during development. *Eukaryot. Cell* **14**, 41–54 (2015).
- P. R. Mayer, N. Huang, C. M. Dewey, D. R. Dries, H. Zhang, G. Yu, Expression, localization, and biochemical characterization of nicotinamide mononucleotide adenylyltransferase 2. *J. Biol. Chem.* **285**, 40387–40396 (2010).
- M. M. Ng, H. C. Dippold, M. D. Buschman, C. J. Noakes, S. J. Field, GOLPH3L antagonizes GOLPH3 to determine Golgi morphology. *Mol. Biol. Cell* **24**, 796–808 (2013).
- J. Rudolf, M. A. Pringle, N. J. Bulleid, Proteolytic processing of QSOX1A ensures efficient secretion of a potent disulfide catalyst. *Biochem. J.* **454**, 181–190 (2013).
- D. Ungar, T. Oka, M. Krieger, F. M. Hughson, Retrograde transport on the COG railway. *Trends Cell Biol.* **16**, 113–120 (2006).
- K. T. Schjoldager, H. Clausen, Site-specific protein O-glycosylation modulates proprotein processing – deciphering specific functions of the large polypeptide GalNAc-transferase gene family. *Biochim. Biophys. Acta* **1820**, 2079–2094 (2012).
- J. C. Nicholson-Fish, A. C. Kokotos, T. H. Gillingwater, K. J. Smillie, M. A. Cousin, VAMP4 is an essential cargo molecule for activity-dependent bulk endocytosis. *Neuron* **88**, 973–984 (2015).
- J. Zhao, B. Li, X. Huang, X. Morelli, N. Shi, Structural basis for the interaction between Golgi reassembly-stacking protein GRASP55 and Golgin45. *J. Biol. Chem.* **292**, 2956–2965 (2017).

22. T. Falguieres, D. Castle, J. Gruenberg, Regulation of the MVB pathway by SCAMP3. *Traffic* **13**, 131–142 (2012).
23. J. J. Jung, S. M. Inamdar, A. Tiwari, A. Choudhury, Regulation of intracellular membrane trafficking and cell dynamics by syntaxin-6. *Biosci. Rep.* **32**, 383–391 (2012).
24. R. L. Nokes, I. C. Fields, R. N. Collins, H. Folsch, Rab13 regulates membrane trafficking between TGN and recycling endosomes in polarized epithelial cells. *J. Cell Biol.* **182**, 845–853 (2008).
25. P. de Graaf, W. T. Zwart, R. A. van Dijken, M. Deneka, T. K. Schulz, N. Geijssen, P. J. Coffer, B. M. Gadella, A. J. Verkleij, P. van der Sluijs, P. M. van Bergen en Henegouwen, Phosphatidylinositol 4-kinasebeta is critical for functional association of rab11 with the Golgi complex. *Mol. Biol. Cell* **15**, 2038–2047 (2004).
26. W. C. Yuan, Y. R. Lee, S. Y. Lin, L. Y. Chang, Y. P. Tan, C. C. Hung, J. C. Kuo, C. H. Liu, M. Y. Lin, M. Xu, Z. J. Chen, R. H. Chen, K33-linked polyubiquitination of Coronin 7 by Cul3-KLHL20 ubiquitin E3 ligase regulates protein trafficking. *Mol. Cell* **54**, 586–600 (2014).
27. S. Conchon, X. Cao, C. Barlowe, H. R. Pelham, Got1p and Sft2p: Membrane proteins involved in traffic to the Golgi complex. *EMBO J.* **18**, 3934–3946 (1999).
28. F. J. del Castillo, M. Cohen-Salmon, A. Charollais, D. Caille, P. D. Lampe, P. Chavrier, P. Meda, C. Petit, Consortin, a trans-Golgi network cargo receptor for the plasma membrane targeting and recycling of connexins. *Hum. Mol. Genet.* **19**, 262–275 (2010).
29. Y. Aoki, R. Manzano, Y. Lee, R. Dafinca, M. Aoki, A. G. L. Douglas, M. A. Varela, C. Sathyaprakash, J. Scaber, P. Barbagallo, P. Vader, I. Mager, K. Ezzat, M. R. Turner, N. Ito, S. Gasco, N. Ohbayashi, S. El Andalousi, S. Takeda, M. Fukuda, K. Talbot, M. J. A. Wood, C9orf72 and RAB7L1 regulate vesicle trafficking in amyotrophic lateral sclerosis and frontotemporal dementia. *Brain* **140**, 887–897 (2017).
30. J. Sasaki, K. Ishikawa, M. Arita, K. Taniguchi, ACBD3-mediated recruitment of PI4KB to picornavirus RNA replication sites. *EMBO J.* **31**, 754–766 (2012).
31. Y. Maeda, T. Ide, M. Koike, Y. Uchiyama, T. Kinoshita, GPHR is a novel anion channel critical for acidification and functions of the Golgi apparatus. *Nat. Cell Biol.* **10**, 1135–1145 (2008).
32. Y. Maeda, T. Kinoshita, The acidic environment of the Golgi is critical for glycosylation and transport. *Methods Enzymol.* **480**, 495–510 (2010).
33. D. L. Gibbons, W. Lin, C. J. Creighton, Z. H. Rizvi, P. A. Gregory, G. J. Goodall, N. Thilaganathan, L. Du, Y. Zhang, A. Pertsemlidis, J. M. Kurie, Contextual extracellular cues promote tumor cell EMT and metastasis by regulating miR-200 family expression. *Genes Dev.* **23**, 2140–2151 (2009).
34. M. DuPage, A. L. Dooley, T. Jacks, Conditional mouse lung cancer models using adenoviral or lentiviral delivery of Cre recombinase. *Nat. Protoc.* **4**, 1064–1072 (2009).
35. F. U. Rutaganira, M. L. Fowler, J. A. McPhail, M. A. Gelman, K. Nguyen, A. Xiong, G. L. Dornan, B. Tavshanjian, J. S. Glenn, K. M. Shokat, J. E. Burke, Design and structural characterization of potent and selective inhibitors of phosphatidylinositol 4 kinase IIIβ. *J. Med. Chem.* **59**, 1830–1839 (2016).
36. H. M. van der Schaar, P. Leyssen, H. J. Thibaut, A. de Palma, L. van der Linden, K. H. Lanke, C. Lacroix, E. Verbeken, K. Conrath, A. M. Macleod, D. R. Mitchell, N. J. Palmer, H. van de Poel, M. Andrews, J. Neyts, F. J. van Kuppeveld, A novel, broad-spectrum inhibitor of enterovirus replication that targets host cell factor phosphatidylinositol 4-kinase IIIβ. *Antimicrob. Agents Chemother.* **57**, 4971–4981 (2013).
37. A. Blagoveshchenskaya, F. Y. Cheong, H. M. Rohde, G. Glover, A. Knodler, T. Nicolson, G. Boehmelt, P. Mayinger, Integration of Golgi trafficking and growth factor signaling by the lipid phosphatase SAC1. *J. Cell Biol.* **180**, 803–812 (2008).
38. T. R. Graham, C. G. Burd, Coordination of Golgi functions by phosphatidylinositol 4-kinases. *Trends Cell Biol.* **21**, 113–121 (2011).
39. K. Hirschberg, C. M. Miller, J. Ellenberg, J. F. Presley, E. D. Siggia, R. D. Phair, J. Lippincott-Schwartz, Kinetic analysis of secretory protein traffic and characterization of golgi to plasma membrane transport intermediates in living cells. *J. Cell Biol.* **143**, 1485–1503 (1998).
40. C. Esselens, J. Malapeira, N. Colomé, C. Casal, J. C. Rodriguez-Manzaneque, F. Canals, J. Arribas, The cleavage of semaphorin 3C induced by ADAMTS1 promotes cell migration. *J. Biol. Chem.* **285**, 2463–2473 (2010).
41. M. R. Wilson, A. Zoubeidi, Clusterin as a therapeutic target. *Expert Opin. Ther. Targets* **21**, 201–213 (2017).
42. M. B. Hampton, K. A. Vick, J. J. Skoko, C. A. Neumann, Peroxiredoxin involvement in the initiation and progression of human cancer. *Antioxid. Redox Signal.* **28**, 591–608 (2018).
43. V. Arpino, M. Brock, S. E. Gill, The role of TIMPs in regulation of extracellular matrix proteolysis. *Matrix Biol.* **44–46**, 247–254 (2015).
44. W. Zeiger, D. Ito, C. Swetlik, M. Oh-hora, M. L. Villereal, G. Thinakaran, Stanniocalcin 2 is a negative modulator of store-operated calcium entry. *Mol. Cell. Biol.* **31**, 3710–3722 (2011).
45. J. C. Lopez-Rodriguez, F. J. Martinez-Carmona, I. Rodriguez-Crespo, M. A. Lizarbe, J. Turnay, Molecular dissection of the membrane aggregation mechanisms induced by monomeric annexin A2. *Biochim. Biophys. Acta* **1865**, 863–873 (2018).
46. L. Sciotti, A. Chiapparino, F. De Giorgi, M. Fumagalli, L. Khoriauli, S. Nergadze, S. Basu, V. Olieric, L. Cucca, B. Banushi, A. Profumo, E. Giulotto, P. Gissen, F. Forneris, Molecular architecture of the multifunctional collagen lysyl hydroxylase and glycosyltransferase LH3. *Nat. Commun.* **9**, 3163 (2018).
47. C. Dayer, I. Stamenkovic, Recruitment of matrix metalloproteinase-9 (MMP-9) to the fibroblast cell surface by lysyl hydroxylase 3 (LH3) triggers transforming growth factor-β (TGF-β) activation and fibroblast differentiation. *J. Biol. Chem.* **290**, 13763–13778 (2015).
48. H. W. Jackson, V. Defamie, P. Waterhouse, R. Khokha, TIMPs: Versatile extracellular regulators in cancer. *Nat. Rev. Cancer* **17**, 38–53 (2017).
49. C. Gaggioli, S. Hooper, C. Hidalgo-Carcedo, R. Grosse, J. F. Marshall, K. Harrington, E. Sahai, Fibroblast-led collective invasion of carcinoma cells with differing roles for RhoGTPases in leading and following cells. *Nat. Cell Biol.* **9**, 1392–1400 (2007).
50. B. M. Emerling, J. B. Hurov, G. Poulogiannis, K. S. Tsukazawa, R. Choo-Wing, G. M. Wulf, E. L. Bell, H. S. Shim, K. A. Lamia, L. E. Rameh, G. Bellinger, A. T. Sasaki, J. M. Asara, X. Yuan, A. Bullock, G. M. Denicola, J. Song, V. Brown, S. Signoretti, L. C. Cantley, Depletion of a putatively druggable class of phosphatidylinositol kinases inhibits growth of p53-null tumors. *Cell* **155**, 844–857 (2013).
51. H. B. Pearson, J. Li, V. S. Meniel, C. M. Fennell, P. Waring, K. G. Montgomery, R. J. Rebello, A. A. Macpherson, S. Koushyar, L. Furic, C. Cullinan, R. W. Clarkson, M. J. Smalley, K. J. Simpson, T. J. Pessesse, P. R. Shepherd, P. O. Humbert, O. J. Sansom, W. A. Phillips, Identification of *Pik3ca* mutation as a genetic driver of prostate cancer that cooperates with *pten* loss to accelerate progression and castration-resistant growth. *Cancer Discov.* **8**, 764–779 (2018).
52. J. Li, Z. Gao, D. Zhao, L. Zhang, X. Qiao, Y. Zhao, H. Ding, P. Zhang, J. Lu, J. Liu, H. Jiang, C. Luo, C. Chen, PI-273, a substrate-competitive, specific small-molecule inhibitor of PI4KIIα, inhibits the growth of breast cancer cells. *Cancer Res.* **77**, 6253–6266 (2017).
53. E. Tokuda, T. Itoh, J. Hasegawa, T. Ijuin, Y. Takeuchi, Y. Irino, M. Fukumoto, T. Takenawa, Phosphatidylinositol 4-phosphate in the Golgi apparatus regulates cell-cell adhesion and invasive cell migration in human breast cancer. *Cancer Res.* **74**, 3054–3066 (2014).
54. N. L. Solimini, J. Luo, S. J. Elledge, Non-oncogene addiction and the stress phenotype of cancer cells. *Cell* **130**, 986–988 (2007).
55. P. Nasarre, R. M. Gemmill, H. A. Drabkin, The emerging role of class-3 semaphorins and their neuropilin receptors in oncology. *Onco. Targets Ther.* **7**, 1663–1687 (2014).
56. I. P. Trougakos, The molecular chaperone apolipoprotein J/clusterin as a sensor of oxidative stress: Implications in therapeutic approaches—A mini-review. *Gerontology* **59**, 514–523 (2013).
57. P. H. Kim, S. S. Na, B. Lee, J. H. Kim, J. Y. Cho, Stanniocalcin 2 enhances mesenchymal stem cell survival by suppressing oxidative stress. *BMB Rep.* **48**, 702–707 (2015).
58. L. C. Gomes-da-Silva, L. Zhao, L. Bezu, H. Zhou, A. Sauvat, P. Liu, S. Durand, M. Leduc, S. Souquere, F. Loos, L. Mondragon, B. Sveinbjörnsson, Ø. Rekdal, G. Boncompain, F. Perez, L. G. Arnaut, O. Kepp, G. Kroemer, Photodynamic therapy with redaporfin targets the endoplasmic reticulum and Golgi apparatus. *EMBO J.* **37**, e98354 (2018).
59. X. Tan, P. Banerjee, X. Liu, J. Yu, D. L. Gibbons, P. Wu, K. L. Scott, L. Diao, X. Zheng, J. Wang, A. Jalali, M. Suraokar, J. Fujimoto, C. Behrens, X. Liu, C. G. Liu, C. J. Creighton, I. I. Wistuba, J. M. Kurie, The epithelial-to-mesenchymal transition activator ZEB1 initiates a prometastatic competing endogenous RNA network. *J. Clin. Invest.* **128**, 3198 (2018).
60. E. M. Johnson, R. E. Price, J. M. Kurie, B. S. Rivera, D. D. Cody, A new method for respiratory gating during microcomputed tomography of lung in mice. *J. Am. Assoc. Lab. Anim. Sci.* **47**, 46–56 (2008).
61. C. J. Creighton, D. L. Gibbons, J. M. Kurie, The role of epithelial-mesenchymal transition programming in invasion and metastasis: A clinical perspective. *Cancer Manag. Res.* **5**, 187–195 (2013).
62. D. K. Mishra, C. J. Creighton, Y. Zhang, F. Chen, M. J. Thrall, M. P. Kim, Ex vivo four-dimensional lung cancer model mimics metastasis. *Ann. Thorac. Surg.* **99**, 1149–1156 (2015).
63. D. K. Mishra, C. J. Creighton, Y. Zhang, D. L. Gibbons, J. M. Kurie, M. P. Kim, Gene expression profile of A549 cells from tissue of 4D model predicts poor prognosis in lung cancer patients. *Int. J. Cancer* **134**, 789–798 (2014).
64. M. Sato, J. E. Larsen, W. Lee, H. Sun, D. S. Shames, M. P. Dalvi, R. D. Ramirez, H. Tang, J. M. DiMaio, B. Gao, Y. Xie, I. I. Wistuba, A. F. Gazdar, J. W. Shay, J. D. Minna, Human lung epithelial cells progressed to malignancy through specific oncogenic manipulations. *Mol. Cancer Res.* **11**, 638–650 (2013).
65. Y. Yang, Y. H. Ahn, Y. Chen, X. Tan, L. Guo, D. L. Gibbons, C. Ungewiss, D. H. Peng, X. Liu, S. H. Lin, N. Thilaganathan, I. I. Wistuba, J. Rodriguez-Canales, G. McLendon, C. J. Creighton, J. M. Kurie, ZEB1 sensitizes lung adenocarcinoma to metastasis suppression by PI3K antagonism. *J. Clin. Invest.* **124**, 2696–2708 (2014).
66. Cancer Genome Atlas Research Network, J. N. Weinstein, E. A. Collisson, G. B. Mills, K. R. Shaw, B. A. Ozenberger, K. Ellrott, I. Shmulevich, C. Sander, J. M. Stuart, The Cancer Genome Atlas Pan-Cancer analysis project. *Nat. Genet.* **45**, 1113–1120 (2013).
67. F. Chen, Y. Zhang, D. L. Gibbons, B. Deneen, D. J. Kwiatkowski, M. Ittmann, C. J. Creighton, Pan-cancer molecular classes transcending tumor lineage across 32 cancer types, multiple data platforms, and over 10,000 cases. *Clin. Cancer Res.* **24**, 2182–2193 (2018).

68. Y. Zhang, L. Yang, M. Kucherlapati, F. Chen, A. Hadjipanayis, A. Pantazi, C. A. Bristow, E. A. Lee, H. S. Mahadeshwar, J. Tang, J. Zhang, S. Seth, S. Lee, X. Ren, X. Song, H. Sun, J. Seidman, L. J. Luquette, R. Xi, L. Chin, A. Protopopov, W. Li, P. J. Park, R. Kucherlapati, C. J. Creighton, A pan-cancer compendium of genes deregulated by somatic genomic rearrangement across more than 1,400 cases. *Cell Rep.* **24**, 515–527 (2018).
69. Y. H. Ahn, D. L. Gibbons, D. Chakravarti, C. J. Creighton, Z. H. Rizvi, H. P. Adams, A. Pertsemlidis, P. A. Gregory, J. A. Wright, G. J. Goodall, E. R. Flores, J. M. Kurie, ZEB1 drives prometastatic actin cytoskeletal remodeling by downregulating miR-34a expression. *J. Clin. Invest.* **122**, 3170–3183 (2012).
70. X. Tan, P. Banerjee, H. F. Guo, S. Ireland, D. Pankova, Y. H. Ahn, I. M. Nikolaidis, X. Liu, Y. Zhao, Y. Xue, A. R. Burns, J. Roybal, D. L. Gibbons, T. Zal, C. J. Creighton, D. Ungar, Y. Wang, J. M. Kurie, Epithelial-to-mesenchymal transition drives a pro-metastatic Golgi compaction process through scaffolding protein PAQR11. *J. Clin. Invest.* **127**, 117–131 (2017).
71. C. L. Grzeskowiak, S. T. Kundu, X. Mo, A. A. Ivanov, O. Zagorodna, H. Lu, R. H. Chapple, Y. H. Tsang, D. Moreno, M. Mosqueda, K. Eterovic, J. J. Fradette, S. Ahmad, F. Chen, Z. Chong, K. Chen, C. J. Creighton, H. Fu, G. B. Mills, D. L. Gibbons, K. L. Scott, In vivo screening identifies GATA2B as a metastasis driver in KRAS-driven lung cancer. *Nat. Commun.* **9**, 2732 (2018).
72. J. J. Brady, C. H. Chuang, P. G. Greenside, Z. N. Rogers, C. W. Murray, D. R. Caswell, U. Hartmann, A. J. Connolly, E. A. Sweet-Cordero, A. Kundaje, M. M. Winslow, An arntl2-driven secretome enables lung adenocarcinoma metastatic self-sufficiency. *Cancer Cell* **29**, 697–710 (2016).
73. M. O. Aksoy, V. Kim, W. D. Cornwell, T. J. Rogers, B. Kosmider, K. Bahmed, C. Barrero, S. Merali, N. Shetty, S. G. Kelsen, Secretion of the endoplasmic reticulum stress protein, GRP78, into the BALF is increased in cigarette smokers. *Respir. Res.* **18**, 78 (2017).
74. S. Das, S. Yu, R. Sakamori, P. Vedula, Q. Feng, J. Flores, A. Hoffman, J. Fu, E. Stypulkowski, A. Rodriguez, R. Dobrowski, A. Harada, W. Hsu, E. M. Bonder, M. P. Verzi, N. Gao, Rab8a vesicles regulate Wnt ligand delivery and Paneth cell maturation at the intestinal stem cell niche. *Development* **142**, 2147–2162 (2015).
75. J. Lee, Y. Xu, T. Zhang, L. Cui, L. Saidi, Y. Ye, Secretion of misfolded cytosolic proteins from mammalian cells is independent of chaperone-mediated autophagy. *J. Biol. Chem.* **293**, 14359–14370 (2018).
76. H. F. Guo, C. L. Tsai, M. Terajima, X. Tan, P. Banerjee, M. D. Miller, X. Liu, J. Yu, J. Byemerwa, S. Alvarado, T. S. Kaoud, K. N. Dalby, N. Bota-Rabassadas, Y. Chen, M. Yamauchi, J. A. Tainer, G. N. Phillips Jr., J. M. Kurie, Pro-metastatic collagen lysyl hydroxylase dimer assemblies stabilized by Fe<sup>2+</sup>-binding. *Nat. Commun.* **9**, 2719 (2018).
77. L. M. Solis, C. Behrens, W. Dong, M. Suraokar, N. C. Ozburn, C. A. Moran, A. H. Corvalan, S. Biswal, S. G. Swisher, B. N. Bekele, J. D. Minna, D. J. Stewart, I. I. Wistuba, Nrf2 and Keap1 abnormalities in non-small cell lung carcinoma and association with clinicopathologic features. *Clin. Cancer Res.* **16**, 3743–3753 (2010).
78. J. D. Roybal, Y. Zang, Y. H. Ahn, Y. Yang, D. L. Gibbons, B. N. Baird, C. Alvarez, N. Thilaganathan, D. D. Liu, P. Saintigny, J. V. Heymach, C. J. Creighton, J. M. Kurie, miR-200 inhibits lung adenocarcinoma cell invasion and metastasis by targeting Flt1/VEGFR1. *Mol. Cancer Res.* **9**, 25–35 (2011).
79. J. L. Albritton, J. D. Roybal, S. J. Paulsen, N. Calafat, J. A. Flores-Zaher, M. C. Farach-Carson, D. L. Gibbons, J. S. Miller, Ultrahigh-throughput generation and characterization of cellular aggregates in laser-ablated microwells of poly(dimethylsiloxane). *RSC Adv.* **6**, 8980–8991 (2016).

**Acknowledgments:** We thank F. Chen for technical assistance. We thank J. Lippincott-Schwartz (Janelia Research Campus), P. Mayinger (Oregon Health & Science University), and T. Balla (NIH) for sharing plasmids. **Funding:** This work was supported by the NIH through R01 CA181184 (to J.M.K.), R01 CA211125 (to J.M.K.), R01AI099245 (to J.S.G.), U19AI109662 (to J.S.G.), P30 CA125123 (to C.J.C.), K99 CA225633 (to H.-F.G.), NIH Lung Cancer SPORE grant P50 CA70907 (to J.M.K. and I.I.W.), Lung Cancer Research Foundation FP#00005299 (to X.T.), and Department of Defense PROSPECT grant W81XWH-07-1-0306 (to I.I.W.). NCI P30 CA16672 Core grant supported flow cytometry. This work was funded by CPRIT-MIRA RP160652. J.M.K. holds the Elza A. and Ina S. Freeman Endowed

Professorship in Lung Cancer. D.H.P. was supported by a CPRIT Graduate Scholar Training Grant (RP140106). D.L.G. is an R. Lee Clark Fellow of the University of Texas MD Anderson Cancer Center, supported by the Jeanne F Shelby Scholarship Fund. The work was also supported by the generous philanthropic contributions to The University of Texas MD Anderson Lung Cancer Moon Shots Program. E.A.P. is supported by the Stanford ChEM-H Physician Scientist Research Fellowship. **Author contributions:** X.T. conceived, designed, executed, and interpreted cell culture and in vivo experiments. P.B. conceived, designed, executed, and interpreted all of the confocal microscopy experiments to analyze Golgi-PI4P, TGN exit, and vesicular trafficking. E.A.P. assessed the antineoplastic properties of PI4KIIIβ antagonists in cell culture and edited the manuscript. C.L.G. performed invasion assay screens of 1q-encoded genes. X.L. assisted X.T. with in vivo experiments. J.Y. bred and genotyped mice for the development of the autologous tumor model. J.Z. tested PI4KIIIβ antagonists in cell culture. V.Z. assisted P.B. with analysis of confocal microscopic images. N.B.-R. performed CAF coculture assays. L.S. performed the HUVEC tube formation assay. H.-F.G. purified the recombinant PLOD3 proteins. D.Y.D. optimized and carried out digital droplet PCR assays on tumor genomic DNA samples. L.M.S. interpreted histologic findings in the autologous tumor model. B.M. performed immunohistochemical analysis of murine tumor tissues. C.B. provided clinical annotation of the human tumor specimens. M.G.R. performed digital image analysis. I.I.W. supervised the efforts of D.Y.D., L.M.S., B.M., M.G.R., and C.B. B.L.R. and D.H.P. performed flow cytometric analysis of immune cells in tumor tissues and splenocyte coculture assays. D.L.G. supervised the efforts of D.H.P. and B.L.R. K.L.S. optimized conditions for the invasion screen and provided open reading frames for 1q-encoded genes. A.M., J.L.H., and P.H.B. performed the experiments on mice bearing human breast cancer xenografts. J.S.G. provided PI4KIIIβ antagonists, synthesized in his lab in collaboration with K.S., I.C., and M.S. Compounds were characterized by F.U.N.R., K.N., G.L., and K.B. E.A.P. and J.S.G. designed in vivo experiments with the antagonists and, along with K.N., directed and assisted with interpretation of data from those experiments. W.K.R. directed and interpreted mass spectrometry experiments. C.J.C. directed and interpreted bioinformatic analyses. J.M.K. conceived and supervised the project and contributed to the design and interpretation of all experiments. **Competing interests:** D.L.G. serves on scientific advisory committees for AstraZeneca, GlaxoSmithKline, Sanofi, and Janssen; provides consults for Ribon Therapeutics; and has research support from Janssen, Takeda, and AstraZeneca. P.H.B. owns stock in GeneTex (<1% of total stock) and has research support from Breast Cancer Research Foundation. I.I.W. serves on advisory boards for Genentech/Roche, Bristol-Myers Squibb, Medscape, AstraZeneca/Medimmune, HTG Molecular, Merck, GlaxoSmithKline, and MSD and receives research support from Genentech, Oncoplex, HTG Molecular, DepArray, Merck, Bristol-Myers Squibb, Medimmune, Adaptive, Adaptimmune, EMD Serono, Pfizer, Takeda, Amgen, Karus, Johnson & Johnson, Bayer, 4D, Novartis, and PerkinElmer (Akoya). J.M.K. has received consulting fees from Halozyme. P.H.B. was a paid Scientific Advisory Board member for Susan G. Komen in 2017. In this role, he helped set the research priorities for this breast cancer foundation. This activity is unrelated to the current study. All other authors declare that they have no competing interests. **Data and materials availability:** All data associated with this study are present in the paper or the Supplementary Materials.

Submitted 18 March 2019  
Resubmitted 14 August 2019  
Accepted 24 October 2019  
Published 22 January 2020  
10.1126/scitranslmed.aax3772

**Citation:** X. Tan, P. Banerjee, E. A. Pham, F. U. N. Rutaganira, K. Basu, N. Bota-Rabassadas, H.-F. Guo, C. L. Grzeskowiak, X. Liu, J. Yu, L. Shi, D. H. Peng, B. L. Rodriguez, J. Zhang, V. Zheng, D. Y. Duose, L. M. Solis, B. Mino, M. G. Raso, C. Behrens, I. I. Wistuba, K. L. Scott, M. Smith, K. Nguyen, G. Lam, I. Choong, A. Mazumdar, J. L. Hill, D. L. Gibbons, P. H. Brown, W. K. Russell, K. Shokat, C. J. Creighton, J. S. Glenn, J. M. Kurie, PI4KIIIβ is a therapeutic target in chromosome 1q-amplified lung adenocarcinoma. *Sci. Transl. Med.* **12**, eaax3772 (2020).

## PI4KIII# is a therapeutic target in chromosome 1q–amplified lung adenocarcinoma

Xiaochao Tan Priyam Banerjee Edward A. Pham Florentine U. N. Rutaganira Kaustabh Basu Neus Bota Rabassadas Hou-Fu Guo Caitlin L. Grzeskowiak Xin Liu Jiang Yu Lei Shi David H. Peng B. Leticia Rodriguez Jiaqi Zhang Veronica Zheng Dzifa Y. Duose Luisa M. Solis Barbara Mino Maria Gabriela Raso Carmen Behrens Ignacio I. Wistuba Kenneth L. Scott Mark Smith Khanh Nguyen Grace Lam Ingrid Choong Abhijit Mazumdar Jamal L. Hill Don L. Gibbons Powell H. Brown William K. Russell Kevan Shokat Chad J. Creighton Jeffrey S. Glenn Jonathan M. Kurie

*Sci. Transl. Med.*, 12 (527), eaax3772. • DOI: 10.1126/scitranslmed.aax3772

### The secrets of malignant secretion

Cancer cells produce and secrete a variety of proteins that promote tumorigenesis, in a process known as malignant secretion. Tan *et al.* identified a region of chromosome 1 that is often amplified in cancer and plays a key role in malignant secretion. In particular, the authors discovered a mechanism by which a Golgi-associated enzyme called PI4KIII# promotes secretion of proteins involved in lung cancer survival and metastasis. The authors identified and optimized chemical inhibitors of PI4KIII# and then tested their effectiveness at blocking malignant secretion and reducing cancer cells' invasiveness *in vitro* and in multiple mouse models of cancer.

### View the article online

<https://www.science.org/doi/10.1126/scitranslmed.aax3772>

### Permissions

<https://www.science.org/help/reprints-and-permissions>